Chapter 1

INTRODUCTION

1.1 Radar in General

1.1.1 Background

Serious development work on radar began in the 1930s, but the basic idea of radar had its origin in the classical experiments on electromagnetic radiation conducted by German physicist Heinrich Hertz during the late 1880s. Hertz set out to verify experimentally the earlier theoretical work of Scottish physicist James Clerk Maxwell. Maxwell had formulated the general equations of the electromagnetic waves governed by the same fundamental laws but having widely different frequencies. Maxwell's work led to the conclusion that radio waves can be reflected from metallic objects and refracted by a dielectric medium, just as light waves can. Hertz demonstrated these properties in 1888, using radio waves at wavelength of 66 cm (which corresponds to a frequency of about 455MHz) [1].

There was no economic, societal and military need for radar until the early 1930s, when long-range military bombers capable of carrying large payloads were developed. This prompted the major countries of the world to look for a means with which to detect the approach of hostile aircraft.

Most of the countries that developed radar prior to World War-II first experimented with other methods of aircraft detection. These included listening for the acoustic noise of aircraft engines and detecting electrical noise from their ignition. Researchers also experimented with infrared sensors. None of these, however, proved effective [1].

First Military Radars

During the 1930s, efforts to use radio echoes for aircraft detection were initiated independently and simultaneously in eight countries with the prevailing military situation and that already had practical experience with radio technology. The United States, Great Britain, Germany, France, Soviet Union, Italy, the Netherlands, and Japan all began experimenting with radar within about two years of one another and embarked, with varying degrees of motivation and success, on its development for military purposes.

Several of these countries had some form of operational radar equipment in military service at the start of World War-II.

Advances during World War-II

The opening of higher frequencies to radar, with its attendant advantages, came about in late 1939 when the cavity magnetron oscillator was invented by British physicist at the University of Birmingham. In 1940 the British generously disclosed to the United States the concept of the magnetron, which then became the basis for work undertaken by the newly formed Massachusetts Institute of Technology (MIT) Radiation Laboratory at Cambridge. It was the magnetron that made microwave radar a reality in World War-II [2].

Radar in the Digital Age

During the 1970s digital technology underwent a tremendous advance, which made practical the signal and data processing required for modern radar. Significant advances also were made in airborne pulse Doppler radar, greatly enhancing its ability to detect aircraft in the midst of heavy ground clutter. The U.S Air Force's airborne-warning-and-control-system (AWACS) radar and military airborne-intercept radar depend on the Doppler principle. It might be noted too that radar began to be used in spacecraft for remote sensing of the environment during the 1970s [3].

1.1.2 Definition

Radar, electromagnetic sensor used for detecting, locating, tracking and recognizing objects of various kinds at considerable distances. It operates by transmitting electromagnetic energy toward objects, commonly referred as targets and observing the echoes returned from them. The targets may be aircraft, sip, spacecraft, automotive vehicles and astronomical bodies or even birds, insects and rain. Besides determining the presence, location and velocity of such objects, radar can sometimes obtain their size and shape as well. What distinguishes radar from optical and infrared sensing device is its ability to detect faraway objects under adverse weather conditions to determine their range or distance with precision.

1.1.3 Radar Classification

According to the configuration variations radars can be classified as following:

- Mono-static and Bi-static radars
- Continuous-wave radar
- Doppler radar
- FM-CW radar
- Mono-pulse radar
- Passive radar
- Planar array radar
- Pulse-Doppler
- Synthetic aperture radar.

According to function radars can be further classified as following:

- Detection and Search radars
- Targeting radar
    - Battlefield and Reconnaissance radar
    - Missile guidance system
    - Target Tracking (TT) System
    - Fire Control (FC) System
    - Airborne Intercept (AI) radars
- Triggers
- Weather radar
- Navigational radar
    - Air traffic Control Navigation
    - Space and Range Instrumentation radar system
- Mapping radar
- Road radar
- Radars for biological research

1.2 Continuous Wave (CW) and Pulsed Radars

1.2.1 CW Radar

Continuous-wave radar systems are those which use a stable frequency continuous wave for transmission and reception [4].

The main advantages of the CW radars are:

- Simple to manufacture.
- No minimum or maximum range (broadcast power level imposes a practical limit on range).
- Maximize power on a target due to continuous broadcasting.

However they also have the following disadvantages:

- They can only detect moving targets, as stationary targets (along the line of sight) will not cause a Doppler shift.

- They cannot measure range. Range is normally measured by timing the delay between a pulse being sent and received, but as CW radars are always broadcasting, there is no delay to measure. Ranging can be implemented, however, by use of a technique known as frequency modulated continuous-wave radar.

1.2.2 Pulsed Radar

Pulsed radars use a train of pulsed waveforms with modulation. Basing on pulse repetition frequency or PRF (Pulse radar frequency). Pulsed radars are classified as low PRF, medium PRF and high PRF. Low PRF radars are used primarily for ranging where target velocity is not needed. High PRF radars are used for measuring target velocity (Doppler shift).

1.3 Radar Terminologies

1.3.1 PRF

Pulsed radars use a train of pulse for transmission and reception as illustrated Figure 1.1. The time interval between any two transmitted pulses is known as the Pulse Repetition

Interval (PRI) on Inter Pulse Period (IPP) denoted by T. The inverse of PRI is called Pulse Repetition Frequency (PRF) denoted by f_r.

During each PRI radar radiates energy only for τ (pulse width) seconds and listens for target returns for rest of the PRI. Here

$$f_r = \frac{1}{PRI} = \frac{1}{T} \tag{1.1}$$

The radar transmitting duty cycle is

$$d_t = \frac{\tau}{T} \tag{1.2}$$

And the radar average transmitted power is

$$P_{avr} = P_t \times d_t \tag{1.3}$$

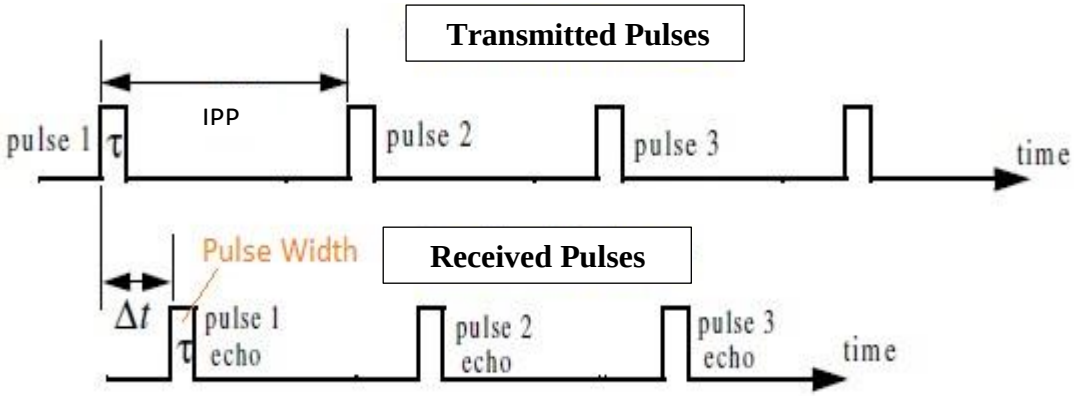

Figure 1.1: PRF and IPP

From the above equations it is clear that increasing the pulse width means increasing the transmitting duty cycle which in turn increases the radar average transmitted power thereby increasing the SNR.

Figure 1.2 is a plot generated by MATLAB simulation that shows the increase in SNR with the increasing pulse width. When pulse width is increased from 0.15 µsec to 1.7 µsec

the increase in SNR is sufficient to detect the target from a distance of even 150 km instead of 75 km [5].

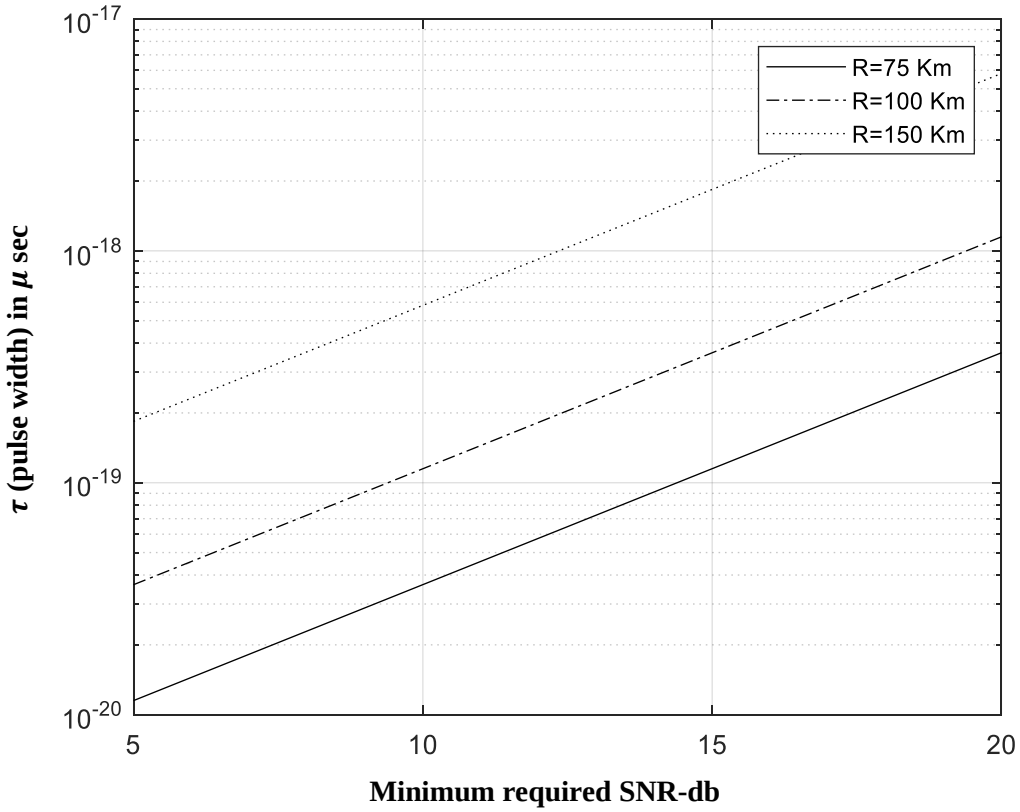

Figure 1.2: Pulse width versus SNR

1.3.2 Maximum Unambiguous Range

Once a pulse is transmitted the radar transmitter must wait for sufficient time for the receiver to receive the echo signal for that particular signal before it sends out the next pulse to avoid ambiguity. Therefore, the maximum unambiguous range (R_u) must correspond to half of PRI.

$$R_u = c\frac{T}{2} = \frac{c}{2f_r} \tag{1.4}$$

1.3.3 Range Resolution

It is the radar's ability to detect targets in close proximity to each other as distinct objects. Radars have a minimum range R_{min} and a maximum range R_{max}. The whole range area is divided into number of range bins or gets (M) each of width ΔR.

Targets separated by at least ΔR can be completely resolved in range. Targets within the same range bin can be resolved in cross range (horizontally) utilizing signal processing techniques. To find the minimum ∆R let us assume two targets are separated by $c\tau/4$ and the radar bandwidth is equal to $1/\tau$, then

$$\Delta R = \frac{c\tau}{2} = \frac{c}{2B} \tag{1.5}$$

In general, radar users and designers alike seek to minimize in order to enhance the radar performance. As suggested by Eq. 1.5, in order to achieve fine range resolution one must minimize the pulse width. However, this will reduce the average transmitted power and increase the operating bandwidth. Achieving fine range resolution while maintaining adequate average transmitted power can be accomplished by using pulse compression techniques.

1.3.4 Doppler Shift

Doppler sift is an apparent change in frequency (or wavelength) due to the relative motion of two objects. When the objects are approaching each other, the Doppler shift causes a shortening of wavelength or increase in frequency. When the two objects are moving away from each other, the Doppler shift causes lengthening of wavelength or decrease in frequency. For a Doppler radar system to measure speed, an accurate sample of the original phase of the transmitted signal must be maintained for comparison against the reflected signal.

For fixed radar with moving target

$$f_D = 2 * V_T * cos\theta * \frac{f_T}{c} \tag{1.6a}$$

For moving radar with moving target

$$f_D = 2 * (V_T + V_R) * cos\theta * \frac{f_T}{c} \quad (1.6b)$$

Where,

f_D = Doppler frequency
f_T = Transmitted frequency
V_T = Target velocity
V_R = Radar velocity
c = speed of light

1.4 Radar Cross Section

Radar Cross Section (RCS) is a parameter that relates the radar to its measure of detectability of a target. In simple words the value of RCS is a measure of how detectable a target is. It is a measure of the ratio of backscatter density in the direction of the radar (from the target) to the power density that is intercepted by the target [6].

1.5 Concept of Stealth & Radar Cross Section (RCS)

The use of the word stealth in the aerospace industry is a fairly recent occurrence. But it falls under a larger program that the military has been studying for a number of years- Low observability or LO technology. Most of the emphasis has been placed on the stealth or LO aircraft is to evade radar detection and rightly so, but to be truly stealthy, six areas must be taken into account. Infrared or heat signature of the aircraft, acoustics or how much noise aircraft makes, visual appearance, smoke emitted, contrails and radar cross section. Although all the others are important, dependence on high-tech radar for air defense makes the RCS, by far the most important area [7].

1.6 Literature Review

In the recent past, research papers regarding RCS analysis of rough and complex targets have been studied and regarding radar cross section some international papers are summarized in this thesis work. [12] presents single and bistatic RCS measurement of stealth aircraft in X band for HH and VV polarization using FEKO software, [26] presents terahertz band has a higher resolution EM wave than Ka band for some certain rough targets, [27] represents the RCS modeling and measurements of automotive applications of several complex targets in anechoic chamber which can be detected on radar by applying Physical Optics method in W band, [28] summarizes on the estimation of Asphalt Reflectivity and measurement of radar cross section of Foreign Object Debris (FOD) using vector network analyzer, [29] exhibits measurement of MRCS of a stealth aircraft based on the variation of incident angle, its polarization, target azimuth angle, elevation angle, [30] presents the Radar Cross Section (RCS) of a CAD model of the stealth bomber B-2 Spirit and results from simulations with the aircraft model. The objective was to investigate how the shape can affect the RCS of an aircraft and how the use of RAM can further reduce its RCS, [31] presents a wire model of a commercial Boeing 747-200 aircraft. The reliability of this model has been assessed by comparing the results given by NEC with the measurements made in an anechoic chamber, also the RCS variation of an aircraft along different flight routes have been investigated here, [32] presents a proper investigation of the RCS of two aircraft in the HF frequency range. A method is also given for deriving an FDTD cell model of a fully three-dimensional aircraft (Navajjo). Similarity between a generic simple aircraft and Navajjo is also shown, [34] presents and analyze a generic airplane design with stealth characteristics using theoretical and experimental tools. Generally, plotting the radar signature of is a complex and challenging work. Especially radar signature of steal aircrafts is rare apart from the manufacturer's classified data.

1.7 Objectives of Research

The objectives of our research work are as follows:

- To understand the analytical basis of research work for F-117A Nighthawk Stealth Aircraft.

- To study and understand RCS dependency on frequency, aspect angle and materials.
- To study and understand the concept of stealth aircraft.
- To improve the RCS measurement through software simulation.
- To evaluate the variation of RCS for different shaped objects and its effects over radar performance.

Chapter 2

PRINCIPLES OF RADAR SYSTEM

2.1 Basic Principle of Radar

Electronic Radar operation principle is very similar to the principle of sound wave reflection. If we shout out loud in the direction of a sound-reflecting object, we'll hear echo. We can then estimate the distance and general direction of the object, if we know the speed of the sound in air. The time required for an echo to return can be roughly converted to distance if the speed of sound is known.

Electromagnetic energy pulses. The Radio-frequency (RF) energy is transmitted to and reflected from the reflecting object. Small portion of the reflected energy is returned to the Radar set. Just as it is in sound terminology, this energy is called an **Echo**. The echo is used by radar sets to determine the direction and distance of the reflecting object.
RADAR is up of the words **Radio Detection and Ranging**. It is refered to electronic equipment that detects the presence of objects by using reflected electromagnetic energy. Under some conditions a radar system can measure the direction, height, distance, course and speed of these objects. Darkness or weather cannot effect the frequency of electromagnetic energy used for radar. Modern radar can extract widely more information from a target's echo signal than its range [6]. But one of its most important function is the calculation of the range by measuring the delay time.

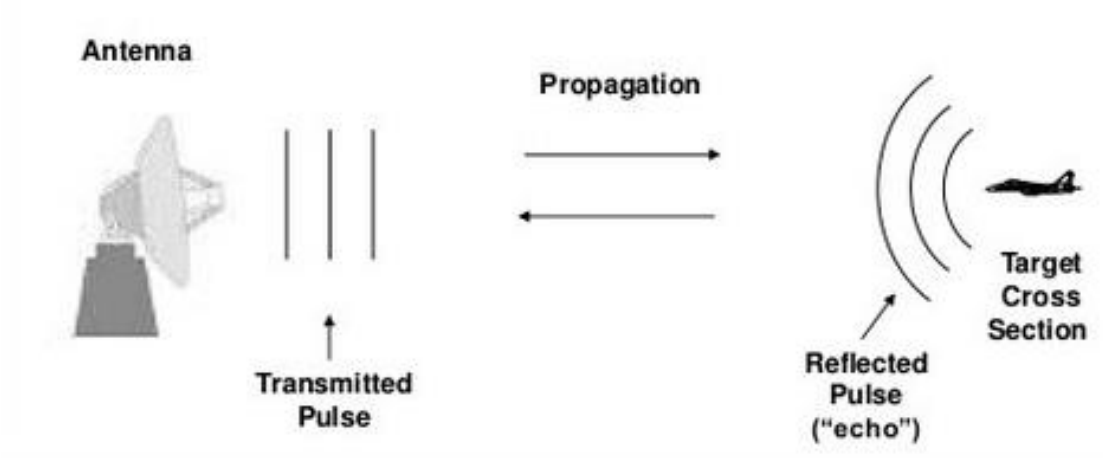

Figure 2.1: Illustration of transmitted and reflected pulses of a RADAR

2.2 RADAR Operation Frequencies

Radar operation frequency is generally selected on the basis of desired detection range, weather and clutter environment, antenna aperture size, properties of targets of interest and cost of RF components.

Different ranges of frequencies from 30MHz to 500MHz are used depending on radar application.

Table 2.1: Radar Frequency Bands

Radar Frequency Bands		
Band Designation	**Frequency Range**	**Typical Usage**
VHF	50-330 MHz.	Very long-range surveillance
UHF	300-1,000 MHz.	Very long-range surveillance
L	1-2 GHz.	Long-range surveillance, enroute traffic control
S	2-4 GHz.	Moderate-range surveillance, terminal traffic control, long-range weather
C	4-8 GHz.	Long-range tracking, airborne weather
X	8-12 GHz.	Short-range tracking, missile guidance, mapping, marine radar, airborne intercept
K_u	12-18 GHz.	High resolution mapping, satellite altimetry
K	18-27 GHz.	Little used (H_20 absorption)
K_a	27-40 GHz.	Very high resolution mapping, airport surveillance
mm	40-100+ GHz.	Experimental

SourceAIAA[8]

2.3 Block Diagram of RADAR

Block diagram of basic radar consists of transmitter, receiver, radar antenna, duplexer and display. Short duration high-power RF pulses of energy that are into space by the antenna is produced by the radar transmitter.

The antenna between the transmitter and receiver is alternately switched by the duplexer so that only one antenna is needed to be used. This switching is necessary because the high-power pulses of the transmitter would destroy the receiver if energy were allowed to enter the receiver [9].

The received RF-signals are amplified and demodulated by the receivers. Video signals are provided by the receiver on the output. Receiver consists of A/D converter, signal processor, IF filter and amplifier, detector.

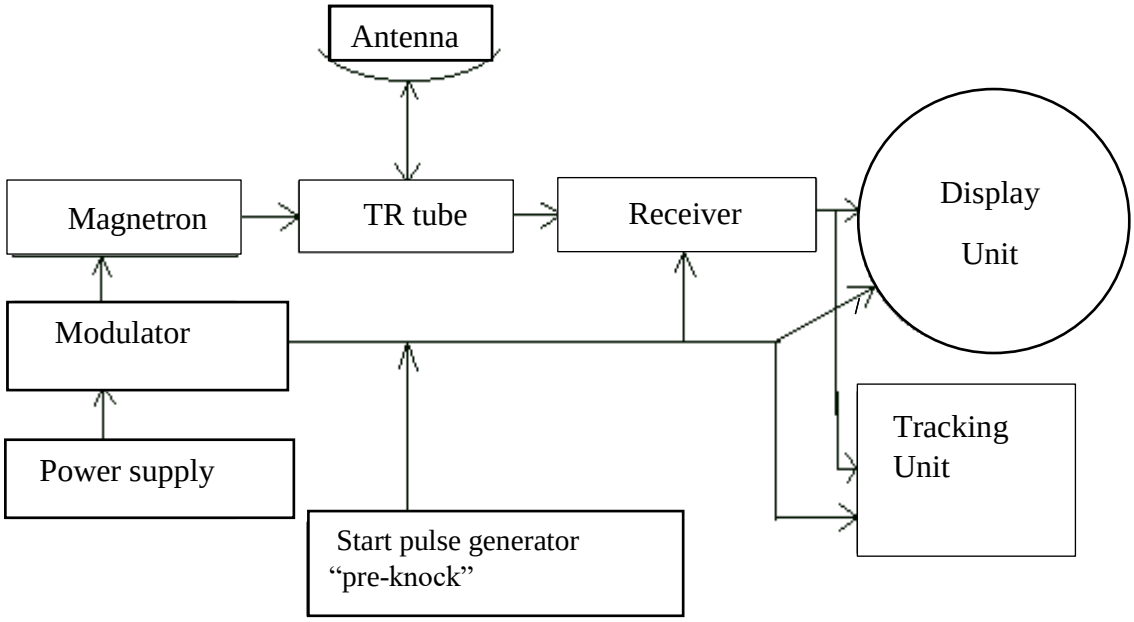

Figure 2.2: Radar Block Diagram

The transmitter energy is transferred to signals in space with the required distribution and efficiency by the antenna. This process is applied in an identical way on reception. A continuous, easily understandable, graphic picture of the relative position of radar targets should be presented to the observer by the display [6].

2.4 Basic Radar Equation

2.4.1 Mono-static Radar Equation

There are many forms of the basic radar equation varying according to the parameters being used. The equation parameters can vary according to the type and configuration of the radar in use. The most common form of the basic radar used in the mono-static radar where the same antenna is used for both transmitting and receiving. The basic radar equation for such mono-static radar system is developed below. Firstly, we considered a noiseless case and then we add the effects of noise to the basic equation.

2.4.2 Noiseless Case

A simple case where the main beam of the radar is only considered the power density at the distance R is

$$S_t = \frac{P_t}{4\pi R^2} \tag{2.1}$$

Where, P_t is total power radiated and R is the radius of the sphere. The total surface area is $4\pi R^2$.

A directional antenna is considered as isotropic antenna is not practically possible. The power density at a point in the space is modified by the power gain of the antenna if a directional antenna is considered instead of isotropic antenna [10]. The power gain is shown by (θ, φ), where θ and φ define the principle plane angles from the main beam of the antenna. The simplest case where the main beam of the radar is only considered the power density at the distance R is

$$S_t = \frac{P_t G_t}{4\pi R^2} \tag{2.2}$$

Where, the power gain G_t of the transmitter antenna is the ratio of the power density of a directive antenna to the power density of the isotropic antenna.

$$G_t = \frac{\text{Power density of directive antenna}}{\text{Power density of isotropic antenna}} \tag{2.3}$$

A portion of the incident power and redirects is intercepted by the target in various direction. Measurement of the amount of incident power intercepted by the target and reflected back in the direction of the radar is defined as radar cross section (RCS) $\boldsymbol{\sigma}$**.**

The radar power density of echo signal is

$$S_r = \frac{s_t \sigma}{4\pi R^2} \tag{2.4}$$

Substituting the value of S_t from (2.2) into equation (2.4) we get

$$S_r = \frac{P_t G_t \sigma}{(4\pi)^2 R^4} \tag{2.5}$$

The power of the echo signal at the radar is effectively intercepted by the receiving antenna over a certain area. This is called the effective area and is denoted by A_e.

Power delivered to the receiver

$$P_r = \frac{P_t G_t \sigma A_e}{(4\pi)^2 R^4} \tag{2.6}$$

The received power by the radar antenna is simply the power density at the antenna multiplied by the effective capture area of the antenna. Considering the antenna gain for more convenience where the gain capture area is related by

$$A_e = \frac{G_r \lambda^2}{4\pi} \tag{2.7}$$

Assuming that the same antenna is used for transmission and reception, so that $G_t = G_r = G$. Then the received power is

$$P_r = \frac{P_t G_t \sigma A_e}{(4\pi)^2 R^4} \tag{2.8}$$

A simple detection of a target in receiver noise, a required detection of a target in receiver noise, a required minimum signal to noise ratio can be defined based on the required detection probability, target statistics and radar characteristics. Receiver noise can be considered to have a constant average power the minimum signal to noise ratio defines the minimum level of received signal that can be tolerated. The maximum detection range is

$$R_{max} = \left[\frac{P_t G^2 \sigma \lambda^2}{(4\pi)^3 P_{min}}\right]^{1/4} \tag{2.9}$$

We can see from the above equation that when all other terms are constant the maximum detection range is varied only as the fourth root of the RCS.

2.4.3 In the Presence of Noise

The returned signal is corrupted by noise which is a function of radar operating bandwidth, B. The input noise power to a lossless antenna is

$$N_i = kT_eB \tag{2.10}$$

Here, T_e is the receiver effective noise temperature. The receiver fidelity is a ability to accurately reproduce, in its output, the signal that appears at its input. The broader the band passed by the frequency selection circuits, the greater is the receiver fidelity. This gives rise to the noise at the receiver input which is defined as the noise figure, F where

$$F = \frac{(SNR)_i}{(SNR)_o} = \frac{\frac{S_i}{N_i}}{\frac{S_o}{N_o}} \tag{2.11}$$

Here S_i and N_i are the input signal and noise power whereas S_o and N_o are output signal and noise power.

Rearranging Eq. 2.11

$$S_i = N_i(SNR)_o = kT_eBF(SNR)_o \tag{2.12}$$

Hence, the minimum detectable signal power can be written as

$$P_{min} = kT_eBF(SNR)_{o_{min}} \tag{2.13}$$

The radar detection threshold is set equal to this minimum output SNR, $(SNR)_{o_{min}}$. Substituting Eq. 2.13 in 2.9 and considering radar losses as L

$$R_{max} = \left(\frac{P_t\sigma G^2\lambda^2}{(4\pi)^3 kT_eBF(SNR)_{o_{min}}}\right)^{1/4} \tag{2.14}$$

Or equivalently,

$$(SNR)_o = \frac{P_t\sigma G^2\lambda^2}{(4\pi)^3 kT_eBFLR^4} \tag{2.15}$$

Eq. 2.15 represents the basic equation for mono-static radar system [10].

2.4.4 How to Increase Range

We can decide on how to increase the radar range by the investigation of the above equations. The effects of RCS are considered in the next chapter. The use of appropriate RCS prediction methods can contribute into exact target detection at longer ranges.

Minimum detectable SNR depends on the threshold level set during radar design. We need to keep it as low as possible to increase the range keeping the false alarm under control.

Range can be increased by increasing transmitted power. As the relationship is proportional hence it will be less effective. Range is increased as square of antenna gain which makes this parameter more effective one.

Increasing wavelength or decreasing operating frequency can increase range [10]. Decreasing operating bandwidth is opposite way to increase the range. Resolution requires bandwidth to be as large as possible.

2.5 Variance of Basic Equation

2.5.1 Bi-static Radar Equation

Transmitting and receiving antennas are used by bi-static radars which are placed in different locations. A synchronization link is necessary between the transmitter and receiver to provide following information:

- The transmitted frequency in order to compute to Doppler shift.
- The transmit time or phase reference in order to measure the total scattered path.

Line-of-sight communications between the transmitter and receiver can maintain frequency and phase reference synchronization. If this is not possible, the receiver may use a stable reference oscillator for synchronization.

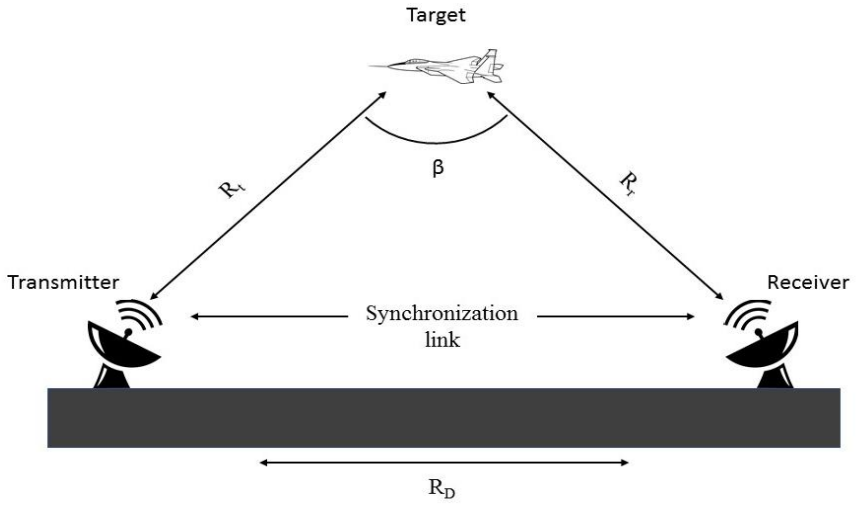

Figure 2.3: Bi-static radar configuration

Figure 2.3 shows the bi-static radar configuration. The angle β is called the bi-static angle. When β approaches 180°, the bi-static RCS becomes very large compared to the mono-static RCS which causes a change in the basic radar equation as given below:

$$P_{Dr} = \frac{P_t G_t G_r \lambda^2 \sigma_B}{(4\pi)^3 R_t^2 R_r^2 L_t L_r L_p} \tag{2.16}$$

Here, a noiseless condition is assumed.

Where,

P_{Dr} = Total power delivered to the signal processor by the receiving antenna

P_t = Peak transmitted power

G_t = Gain of transmitting antenna

G_r = Gain of receiving antenna

R_t = Range from transmitter

R_r = Range from receiver

L_t = Transmitter losses

L_r = Receiver losses

L_p = Medium propagation loss.

2.5.2 Low PRF Radar Equation

Receiving duty factor can be defined as

$$d_r = \frac{T-\tau}{T} = 1 - \tau f_r = 1 - \frac{\tau}{T} \tag{2.17}$$

Foe low PRF(T>> τ), the receiving duty factor $d_r \approx 1$. Ignoring the impact of receiving duty factor low PRF radar equation for n_p coherent pulses $(n_p = T_i f_r)$ can be written as following

$$(SNR)_{n_p} = \frac{P_t G^2 \lambda^2 \sigma T_i f_r}{(4\pi)^3 k T_e B F L R^4} = \frac{P_t G^2 \lambda^2 \sigma T_i f_r \tau}{(4\pi)^3 k T_e F L R^4} \tag{2.18}$$

Here,

T_i= Time on target

B = Bandwidth

Transmission duty factor is negligible compared to the receiving duty factor low PRF radars result in maximum unambiguous range nearby increasing overall range of the radar.

It is already defined time on target $T_i = \frac{n_p}{f_r}$; therefore, as the PRF, f_r is decreased time of the scanning beam on target is increased resulting in better output SNR. As a result low PRF radars give better SNR for targets at longer ranges [10].

2.5.3 High PRF Radar Equation

Central power spectrum line (DC component) for high PRF pulse train contains most of the signal's power. It's value is $(\tau/T)^2$, and it is equal to the square of the transmit duty factor. Thus, using Eq. 2.19, the single pulse radar equation for high PRF radar is

$$(SNR)_o = \frac{P_t G^2 \lambda^2 \sigma d^2}{(4\pi)^3 k T_e B F L R^4 d_r} \tag{2.19a}$$

We cannot ignore d_r since $d_r \approx d_t \approx \tau f_r$ for High PRF radar. For high PRF radar, B=T_i. Additionally, if we replace $P_{avr} = \tau P_t f_r$, then Eq. 2.19a becomes

$$SNR = \frac{P_{avr} T_i G^2 \lambda^2 \sigma}{(4\pi)^3 k T_e F L R^4} \tag{2.19b}$$

Since $P_{avr}T_i$ in Eq. 2.19b is a kind of energy product therefore it indicates that high PRF radars can enhance detection performance by using relatively low power and longer integration time. Low PRF radars are used primarily for ranging where target velocity is not needed. High PRF radars are used for measuring target velocity (Doppler Shift).

2.5.4 Surveillance Radar Equation

A specified volume in space for targets is continuously scanned by surveillance or search radars. Radar take a volume defined by the solid angle if we define T_{sc} as the time. So the basic radar Eq. can be modified which gives us the search radar equation as

$$SNR = \frac{P_{avr}A\sigma T_{sc}}{16R^4kT_eLF\Omega} \tag{2.20}$$

The quantity $P_{avr}A$ in Eq. 2.20 is known as the power aperture product. The power aperture product is widely used to recognize the radar ability to fulfill its search mission. A power aperture product is computed to meet predetermined SNR and radar cross section for a given search volume defined by Ω.

2.6 Variation of Radar Parameters and its Effect on Radar Performances

2.6.1 Effect of RCS and Transmitted Peak Power

We will perform a MATLAB simulation using basic radar equation. We can formulate the following findings if we analyze the generated plots for different parameter changes:

- Doubling the peak power improves SNR only a tittle (3 to 5 dB) in Figure 2.4b.
- Doubling the RCS improves SNR a little better (almost 10 dB) in figure 2.4a. Although both RCS and the transmitted peak power has a linear relationship with SNR, but since increase in RCS indicates increase in the power reflectivity of the target therefore its effect is more prominent.
- Other radar parameters such as antenna gain variation should be considered to improve SNR or detection range effectively.

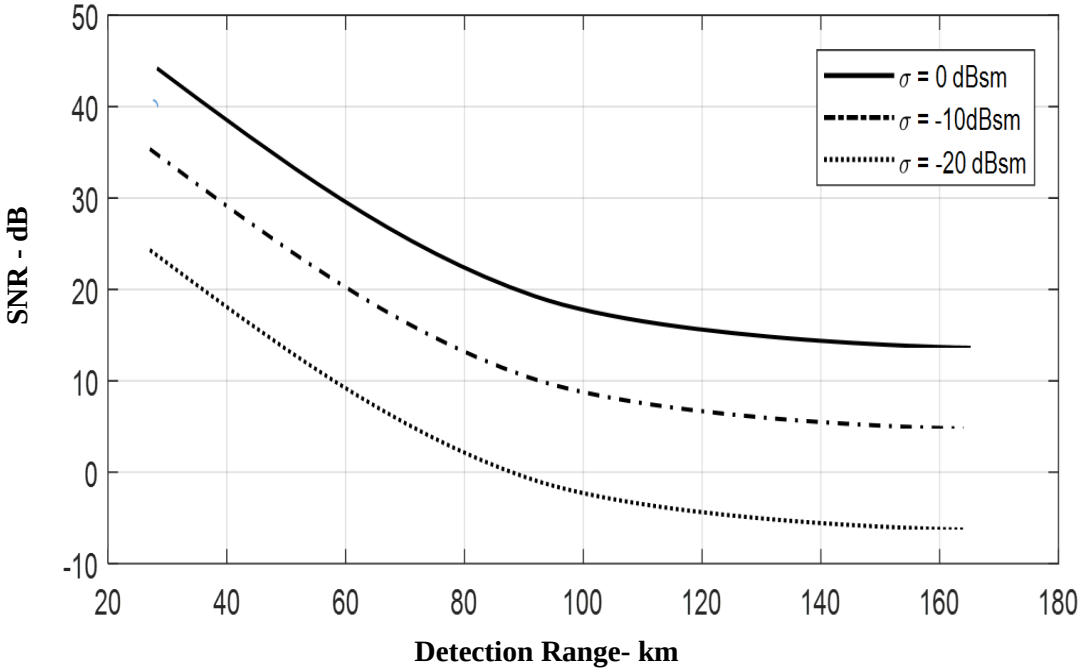

(a)

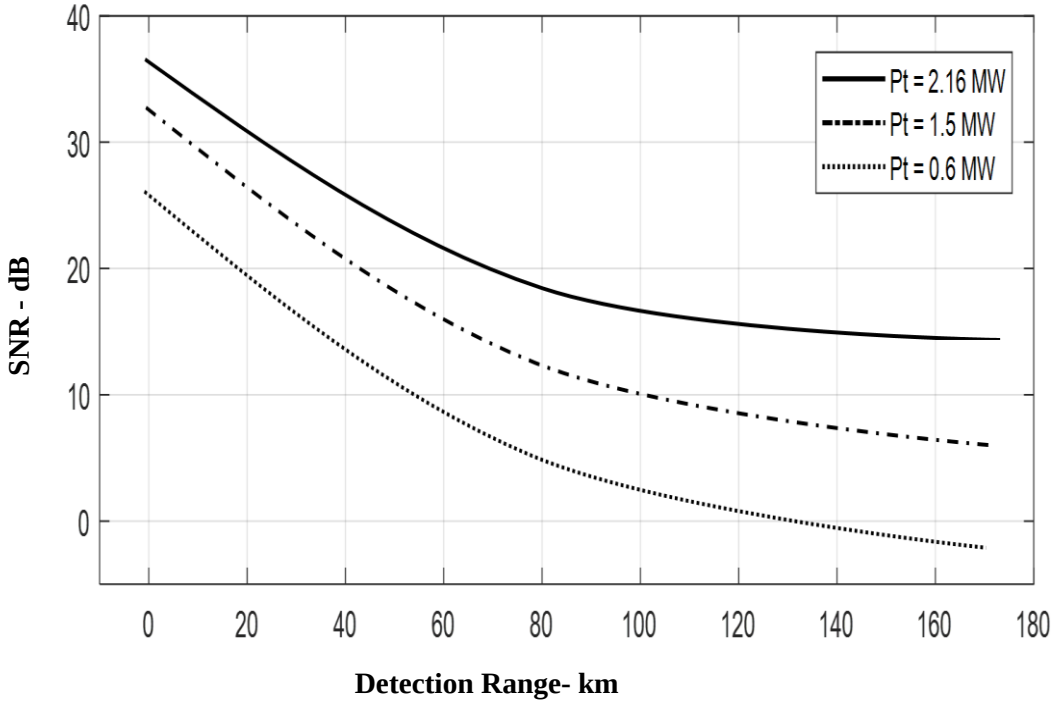

(b)

Figure 2.4: (a) Variation of RCS in improving SNR and detection range. (b) Variation of peak power in improving SNR and detection range [5]

2.6.2 Effect of Changing PRF

Let us perform a MATLAB simulation using radar equation to show the effect PRF on radar performance. We can formulate the following findings for different parameter changes if we analyze the generated plots:

- Integrating a limited number of pulses can significantly enhance the SNR.
- However, integrating large amount of pulses does not provide any further major improvement.
- For any variation of RCS or peak power, the effect of change in PRF remains same.

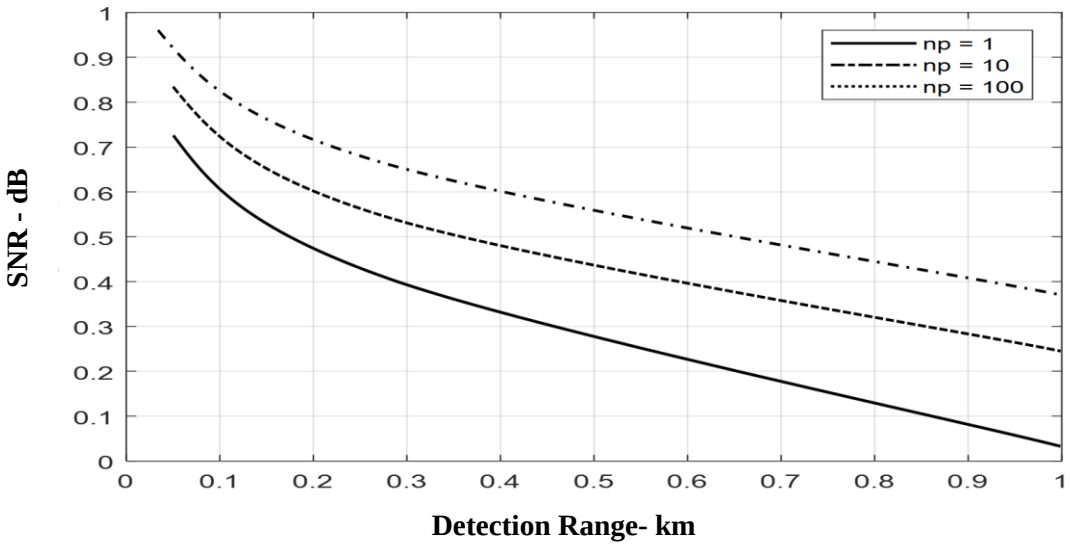

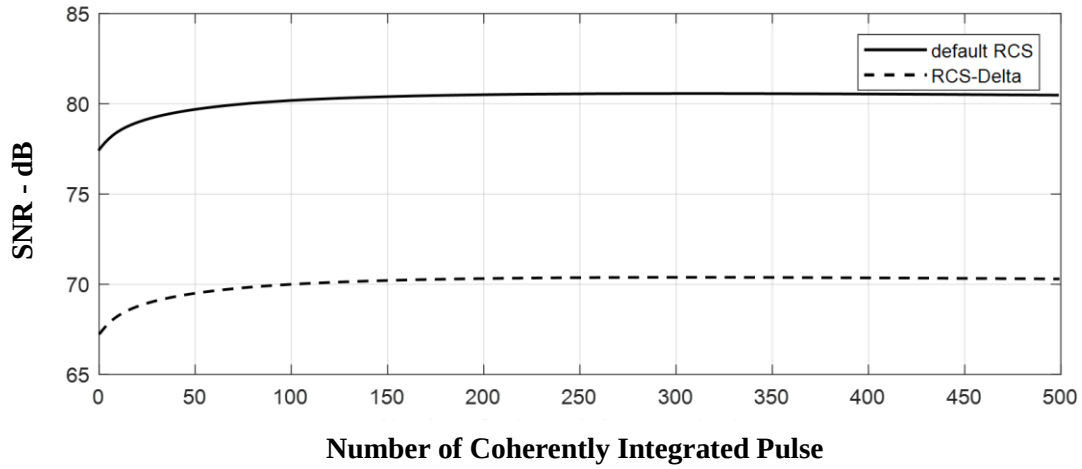

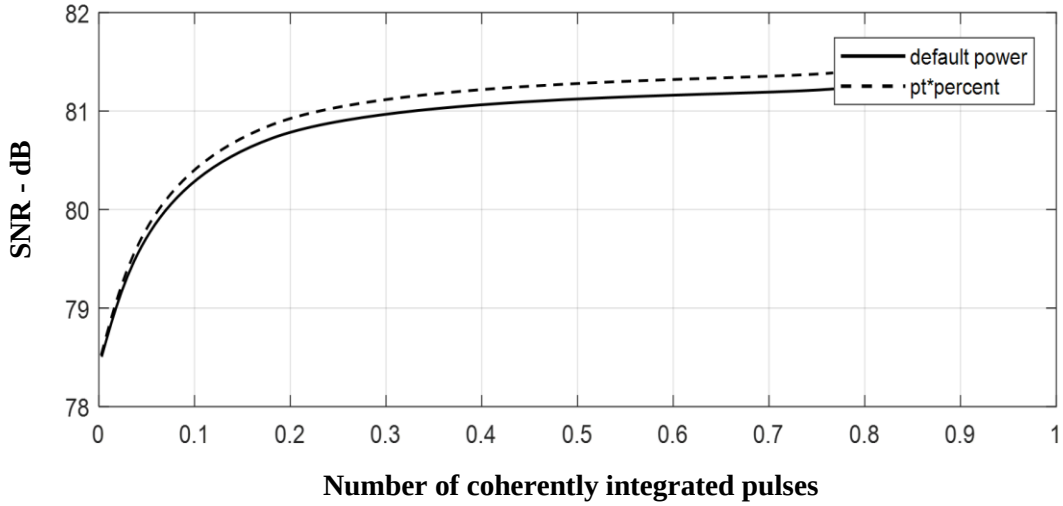

Figure 2.5: Effect of changing PRF on SNR and range [5]

2.6.3 Effect of Power Aperture Product

Let us run a MATLAB simulation that implements the search radar equation. two plots are generated by the simulation. The observation of the plots reveals the following facts:

- It is shown in Figure 2.6a that with the increase of power aperture product, the detection range is also increased for all types of target or RCS sizes. This is because the increase in aperture actually increases the antenna gain.
- It means we can increase the antenna aperture to compensate for the lack of power being transmitted to cover a wider range of area for target detection.
- It is shown in Figure 2.6a that different combination of power and aperture area is possible to detect same targets. It also indicates that for the same maximum radar detection range we have a number of options to choose the desired aperture size and the average transmitted power according to the application of the radar.

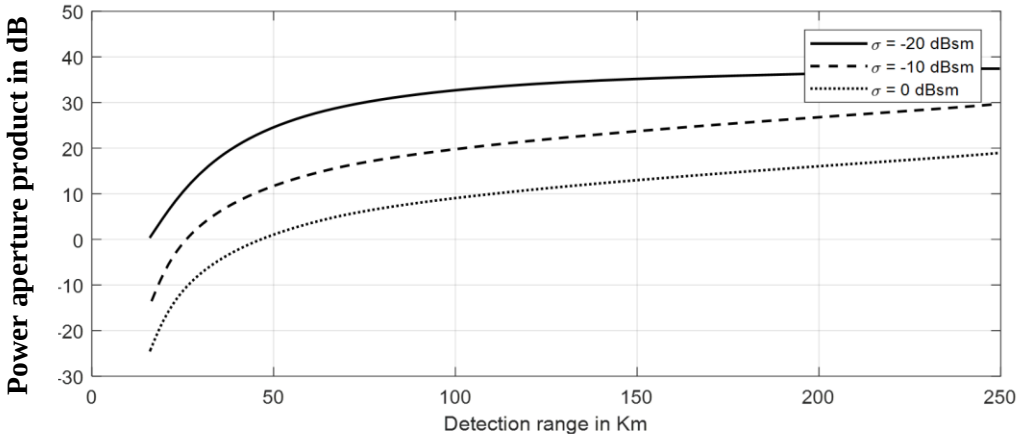

Figure 2.6 (a): Increasing power aperture product to increase detection range [5

Detection range in km

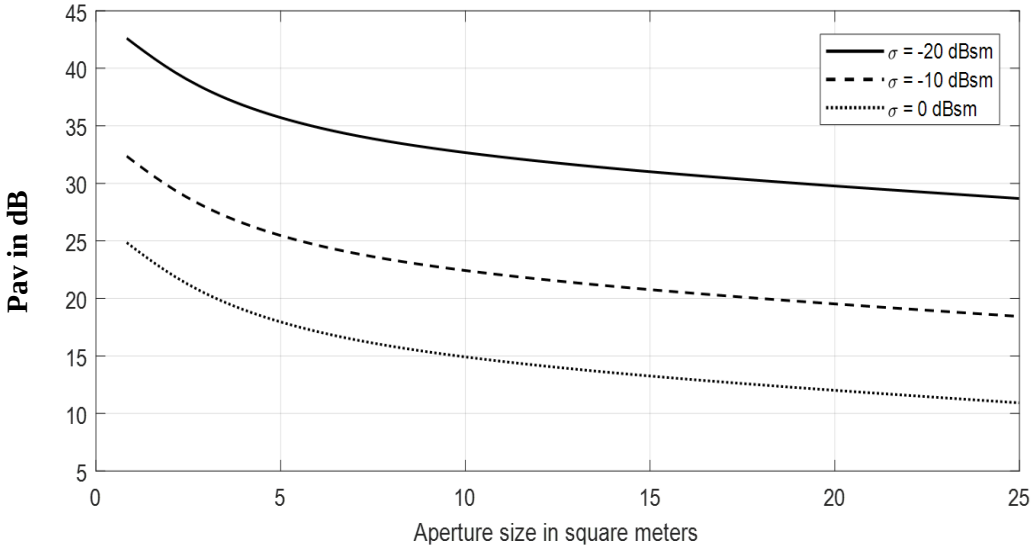

Figure 2.6 (b): Increasing aperture size to decrease average power requirement [5]

Chapter 3

THEORY ON RADAR CROSS SECTION

3.1 Introduction

When electromagnetic waves are incident on any object, the energy spreads in all directions. The spatial distribution of energy depends specially on object geometry, material composition, operation frequency, polarization of incident wave etc. This energy distribution is called *scattering* and the object from where the energy reflects is called a *scatterer.*

Scattered waves are broken down into two polarization specifications. One is waves of same polarization as receiving antenna and the other is of different polarization to which receiving antenna will not respond. The intensity of backscattering energy having same polarization that returns to the source or reflects in a given direction is defined as *Radar Cross Section (RCS)* of target.

When a target is illuminated by RF energy, it acts like an antenna having near field and far field. Near field is the closest region of scatterer. Near field behaviors decay rapidly with distance away from an object whereas in case of far field, radiative field's intensity decays with an inverse square law. However, our concern is to calculate both near and far field of a scatterer to analyze the RCS of a complex target.

3.2 IEEE RCS Definition

IEEE dictionary defines RCS as a measure of reflective strength of a target defined as 4π times the ratio of the power per unit solid angle scattered in a specific direction to the power per unit area in a plane wave incident on a scattered from a specified direction. More precisely it is the limit of the ratio as the distance from the scatterer to the point where the scattered power is measured approaches infinity.

$$\sigma = \lim_{R\to\infty} 4\pi R^2 \frac{|E^{scat}|^2}{|E^{inc}|^2} \tag{3.1}$$

Where, E^{scat} is the scattered electric field and E^{inc} is the field incident at the target [11].

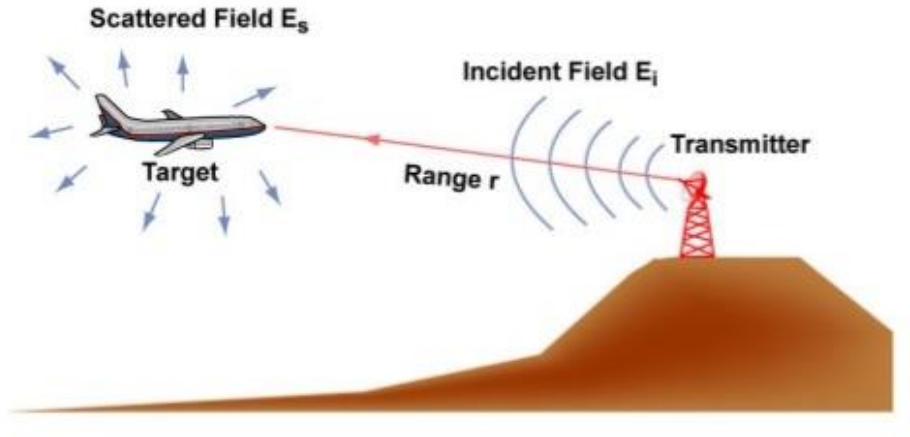

Figure 3.1: Pictorial demonstration of incident and scattered energy

3.3 RCS Derivation

This above definition can be illuminated from the following derivation. Let the incident power density at the target scattering from distant radar be P_i W/m^2. The amount of power intercepted by the target object is related to its cross section σ, that is σP_i. Then the intercepted power is reradiated as the scattered power or absorbed as heat. Assuming power is scattered uniformly in all 4π square of space so that the scattered power density, is given by

$$P_s = \frac{\sigma P_i}{4\pi R^2} \tag{3.2}$$

Now solving this equation for σ,

$$\sigma = 4\pi R^2 \left(\frac{P_s}{P_i}\right) \tag{3.3}$$

Now, considering the distance of radar receiving antenna R which is far from the target to avoid near field effect and so the equation can be modified as

$$\sigma = 4\pi R^2 \lim_{R\to\infty} \left(\frac{P_s}{P_i}\right) \tag{3.4}$$

Similarly,

$$\sigma = 4\pi R^2 \frac{|\,\mathrm{E}^{scat}\,|^2}{|\,\mathrm{E}^{inc}\,|^2} = 4\pi R^2 \frac{|\,\mathrm{H}^{scat}\,|^2}{|\,\mathrm{H}^{inc}\,|^2} \tag{3.5}$$

Because in far field either E or H is sufficient to describe the EM wave [12].

Radar Cross Section is measured in square meters. Due to large dynamic range of RCS a logarithmic power scale is used with reference value of $\sigma_{ref} = 1\ m^2$

$$\sigma_{dBsm} = \sigma_{dBm^2} = 10\log_{10}\left[\frac{\sigma_{m^2}}{\sigma_{ref}}\right] = 10\log_{10}\left[\frac{\sigma_{m^2}}{1}\right] \tag{3.6}$$

Generally, when radar waves are incident on a target, total power is withdrawn by virtue of scattering and absorption to normalize the incident power density. But the target backscattered RCS (σ) is measured from a portion of total power scattered by the target in all 4π square spatial direction. Therefore, total target scattered RCS, σ_T is given by:

$$\sigma_T = \frac{\text{Total scattered power (W)}}{\text{Incident power density (w/m}^2)} \tag{3.7}$$

Assuming spherical coordinate system defined by (r,θ,φ) where at range r, the target scattered cross section is a function of (θ, φ). Let the angle (θ_i,φ_i) represents the direction of propagation of the incident wave and (θ_s, φ_s) defines the direction of propagation of scattered wave [10]. So the σ_T is formally defined by integrating the scattering cross section over all spatial directions scattered around.

$$\sigma_T = \frac{1}{4\pi}\int_0^{\pi}\int_0^{2\pi}\sigma(\theta_s,\varphi_s)\sin\theta d\theta d\varphi \tag{3.8}$$

3.4 Mono-static and Bi-static RCS:

In special cases, when $\theta_s = \theta_i$ and $\varphi_s = \varphi_i$ specifies mono-static RCS in which transmitter and receivers are collocated. RCS measured by radar at angles $\theta_s \neq \theta_i$ and $\varphi_i \neq \varphi_s$ is called bi-static RCS in which transmitter and receiver are in distant location.

.

Mono-static Radar Geometry

Bi-static Radar Geometry

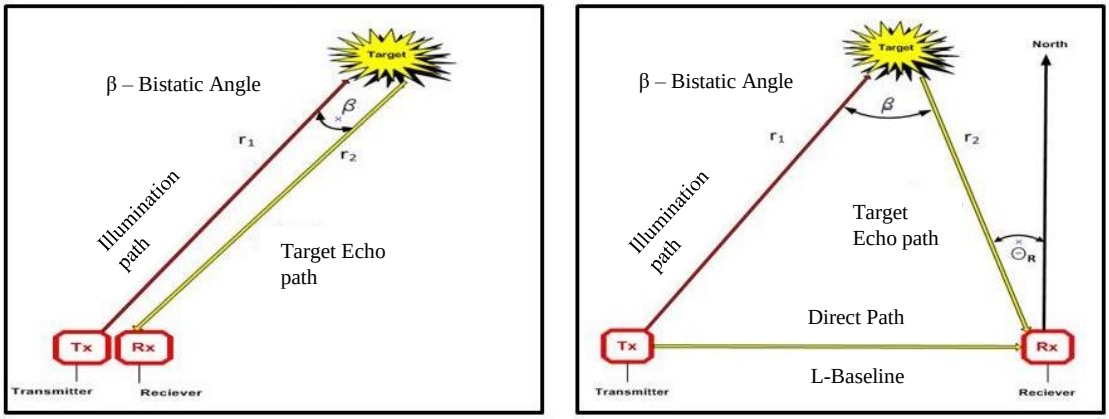

Figure 3.2: RCS for Mono-static and Bi-static scattered field

3.5 Far field Calculations from Maxwell and Stratton-Chu Equation:

The power backscattered from a target in the direction of radar receiver antenna hence radar cross section can be calculated using *Maxwell's equation* with proper boundary condition. When EM wave is incident on a body, the boundary conditions on the fields require surface currents flow. These currents in turns reradiate a scattered EM wave. The strength of the reflected and scattered wave depends on incident polarization and material properties.

Surface fields are characterized by surface electric, magnetic currents and charges. The relation between surface source currents to the scattered fields is described by ***Stratton-Chu*** equation, which is alternate expression of Maxwell's equation.

If two regions are separated by a surface 'S' and if there are magnetic and electric source currents and charges in each region, the field anywhere in region-1 is given as sum of volume integral over the source in region-1 and surface integral over the fields or surface S caused by the sources in region-2.

The Stratton-Chu equation for the scattered E field is

$$E^s = \int_v (-j\omega\mu J\psi - M\times\nabla\psi + \frac{\rho}{\in}\nabla\psi)dV + \oint_s [-j\omega\mu(n\times H)\psi + (n\times E)\times\nabla\psi + (n.E)\nabla\psi]dS \quad (3.9)$$

Corresponding expression for the scattered H field is

$$H^s = \int_v (-j\omega \in M\psi - J \times \nabla\psi + \frac{\rho^*}{\mu}\nabla\psi)dV + \oint_s [-j\omega \in (n \times E)\psi + (n \times H) \times \nabla\psi + (n.\mathrm{H})\nabla\psi]dS \quad (3.10)$$

Where,

$\nabla\psi$ $\cong$ - $jk\hat{s}\,\psi$, is the gradient of Green's function

ψ_0 = $\exp(-jkR_{fs}) / 4\pi R_{fs}$

K = Wave number,

$\hat{s}$ = Unit vector aligned along the scattering direction,

n = Unit normal to the surface,

J = Electric current density

M = Magnetic current density

ρ = Electric charge density

$\rho*$ = Magnetic charge density

$\in$ = Permittivity

μ = Permeability

If we consider ***far-field*** approximation at distance R from the target origin where far-field observation point is taken at infinity but also with a well-defined angular position (θ, φ) the previous Stratton-Chu formula can be simplified. Therefore, simplified Stratton-Chu equation to calculate far electromagnetic field from the near field can be written as [13]

$$\overline{E_s} = ik\psi_0 \int_s \hat{s} \times [n \times \overline{E} - Z_0 \hat{s} \times (n \times \overline{H})] e^{ik\hat{r}.(\bar{i}-\bar{s})} dS \quad (3.11)$$

$$\overline{H_s} = ik\psi_0 \int_s \hat{s} \times [n \times \overline{H} - Y_0 \hat{s} \times (n \times \overline{E})] e^{ik\hat{r}.(\bar{i}-\bar{s})} dS \quad (3.12)$$

Where,

ψ_0 = exp(*ikR)*/4 π *R* = Far field Green's function

$\hat{\boldsymbol{s}}$ = Unit vector aligned along the scattering direction,

$\bar{\boldsymbol{i}}$ = Unit vector along the direction of incidence,

$\hat{\boldsymbol{r}}$ = Position vector from the local origin to the surface patch dS,

Z_0 = $\sqrt{\frac{\mu}{\in}}$ = Impedance of free space,

And Y_0 = $\sqrt{\frac{1}{\boldsymbol{Z}_0}}$ = Admittance of free space.

3.6 Factors That Affects RCS

3.6.1 RCS Dependency over target size

As of general knowledge, the larger the object the greater it's RCS. This is because for a larger size of object, backscattered wave has almost the same strength as incident/scattered wave. Consequently, the radar reflection is stronger which results in larger RCS. Also radar constructed at one band cannot detect other band objects [5].

3.6.2 RCS Dependency on Wavelength

Radar cross section also depends on the characteristics dimensions of the object compared to the radar wavelength. When the wavelength is large compared to the objects dimension, scattering is said to be in Rayleigh region. On the other hand, where the wavelength is small compared to the objects dimensions, it is in the optical region [5].

3.6.3 RCS Dependency on Aspect Angle

RCS surely varies as a function of aspect angle. For any two isotropic scatterers, the composite RCS includes the superposition of the two individual radar cross sections. Taking any one object as phase reference, when the aspect angle is varied, the composite RCS is modified by the phase that corresponds to the electrical spacing between two scatterers, that is

$$Elec - spacing = \frac{2\times 1.0\times \cos(aspectangle)}{\lambda} \quad (3.13)$$

The following figure shows the composite RCS for such two objects. It was simulated using MATLAB [5].

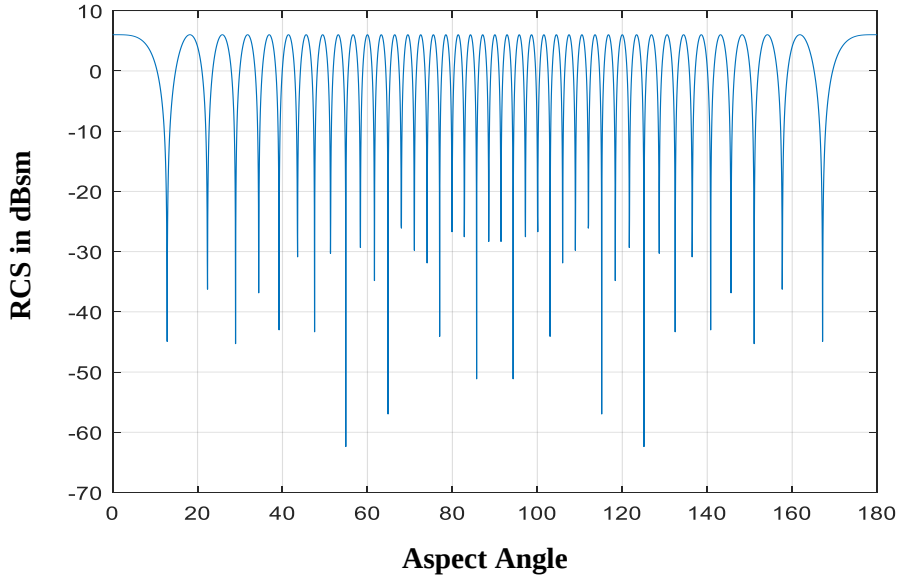

Figure 3.3: RCS dependency on aspect angle of 3GHz frequency and 1m spacing

The figure shows that RCS is highly dependent on radar aspect angle, where the curves represent the composite RCS of two individual scatterers. The other parameters were scat_spacing = 1.0, frequency = 3GHz.

Constructive and destructive interference takes place between the RCS of two individual scatterers depending on the specific aspect angle. When the aspect angle is 0° and 180° constructive interference takes place and the RCS fluctuation is reduced. On the other hand, when the aspect angle is around 90° destructive interference takes place.

3.6.4 RCS Dependency on Frequency

For the demonstration of RCS dependency over frequency, two unity isotropic far field scatterers are aligned with radar line of sight, and the composite RCS is measured by the radar as the frequency is varied from 8 GHz to 12.5 GHz (X-band).

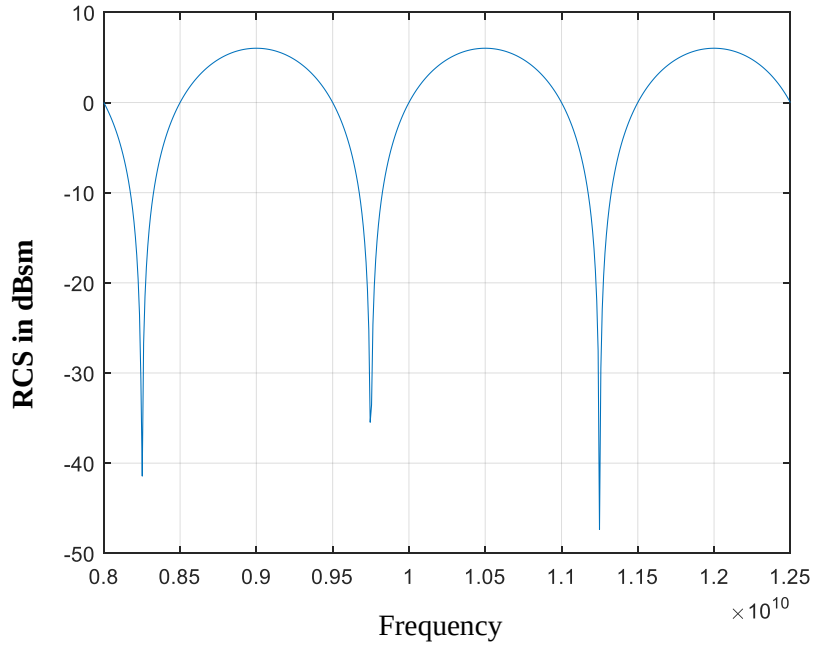

Figure 3.4 (a): RCS dependency on frequency for .1m spacing

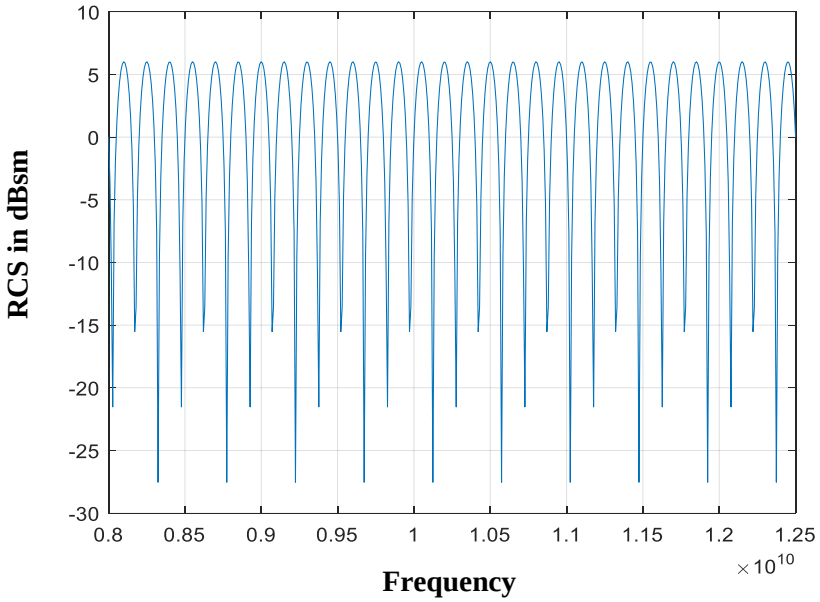

Figure 3.4 (b): RCS dependency on frequency range for 1m spacing

The plots show the RCS dependency on frequency and it also represents the RCS fluctuation as a function of frequency. For little frequency change, serious RCS fluctuation is observed which increase in scattering spacing though from .1 m to 1 m this fluctuation increases at huge rate. So it can be summarized that higher frequency variation produces significant RCS fluctuation at a constant scattering spacing.

3.7 RCS of Simple Objects

The RCS of simple targets can be easily measured using EM theory. As a part of analysis, examples of backscattered radar cross section for a number of simple shaped objects has been studied. In all cases, except for the perfectly conducting sphere, only optical region approximation is presented.

3.7.1 Perfectly Conducting Sphere

The scattered waves from a perfectly conducting sphere are co-polarized (have the same polarization) with the incident waves. This is because of symmetry and results in zero cross-polarization backscattered wave.

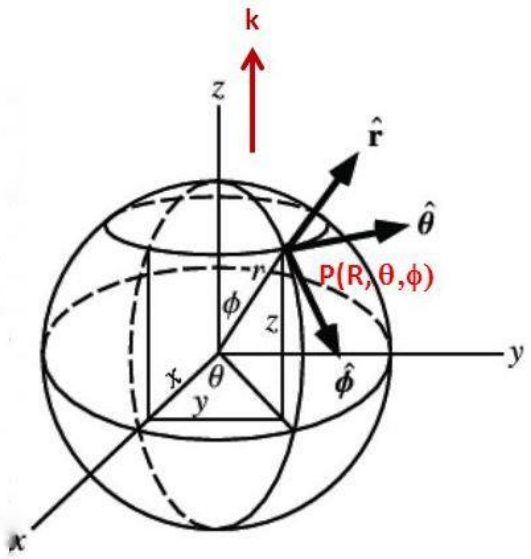

Figure 3.5: Direction of antenna receiving backscattered waves of sphere

The normalized exact backscattered RCS for a perfectly conducting sphere in a Mie series is given by

$$\frac{\sigma}{\pi r^2} = \left(\frac{j}{kr}\right) \sum_{n=1}^{\infty} (-1)^n (2n+1) \left[\left(\frac{krJ_{n-1}(kr) - nJ_n kr}{krH_{n-1}^{(1)}(kr) - nH_n^{(1)}(kr)} \right) - \left(\frac{J_n(kr)}{H_n^{(1)}(kr)} \right) \right] \quad (3.14)$$

Calculation in Mie series is very important from the view point of radar designing. The result of the simulation shows that the backscattered RCS for a perfectly conduction sphere is constant in the optical region. This is the reason why the engineers refer spheres of known cross-section to experiment any radar system capabilities.

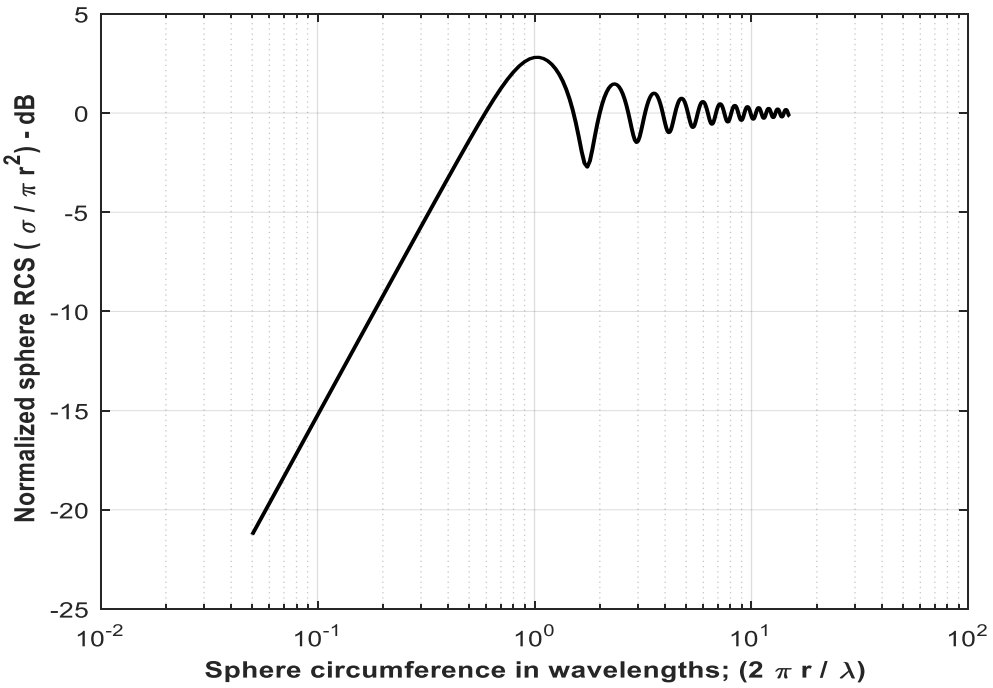

Figure 3.6: Normalized backscattered RCS for a perfectly conducting sphere using semi-log scale

In the above Figure 3.6 three separate regions are evident. They are separated from each other by the horizontal log scale.

Firstly, the Rayleigh region where $r \gg \lambda$

In this case, $\sigma = \pi r^2$

Second, optical region, where $\lambda \gg r$ and $\sigma = 9\pi r^2 (kr)^4$.

And the third one is Mie region, which is a region oscillatory between Rayleigh and optical region.

Where r is the radius of the radius of the sphere. $k = \frac{2\pi}{\lambda}$ and λ is the wavelength.

3.7.2 Circular Flat Plate

The RCS of a circular flat plate target only depends on aspect angle. The backscattered RCS of a circular flat plate has no dependency on ϕ due to the circular symmetry.

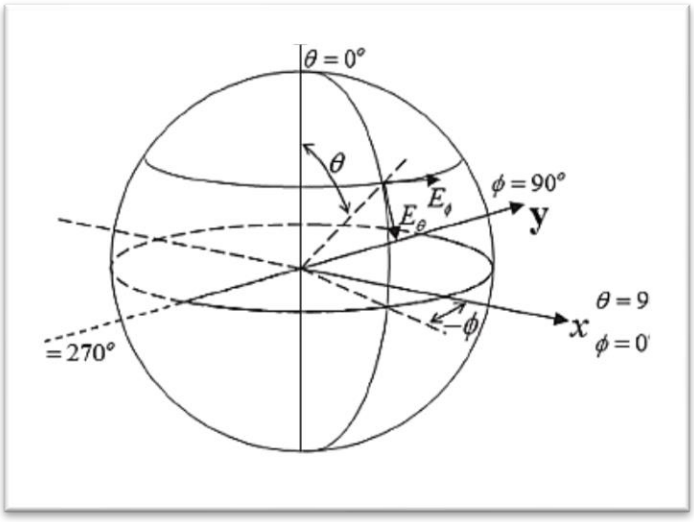

Figure 3.7: Direction of antenna receiving backscattered waves of circular flat plate

For a normal incidence of wave that means zero aspect angle the backscattered RCS for a circular flat plat is given as

$$\sigma = \frac{4\pi^3 r^4}{\lambda^2}\theta = 0° \tag{3.15}$$

For incidence out of 0° two approximations for the circular flat plate backscattered RCS are,

$$\sigma = \frac{\lambda r}{8\pi sin\theta (tan\theta)^2} \tag{3.16}$$

$$\sigma = \pi k^2 r^4 \left(\frac{2J_1(2krsin\theta)}{2krsin\theta}\right)^2 (cos\theta)^2 \tag{3.17}$$

Where $k = \frac{2\pi}{\lambda}$ and J_1 is the first order spherical Bessel function evaluated at β. The simulation is done by MATLAB where r = 0.125m and f = 8GHz.

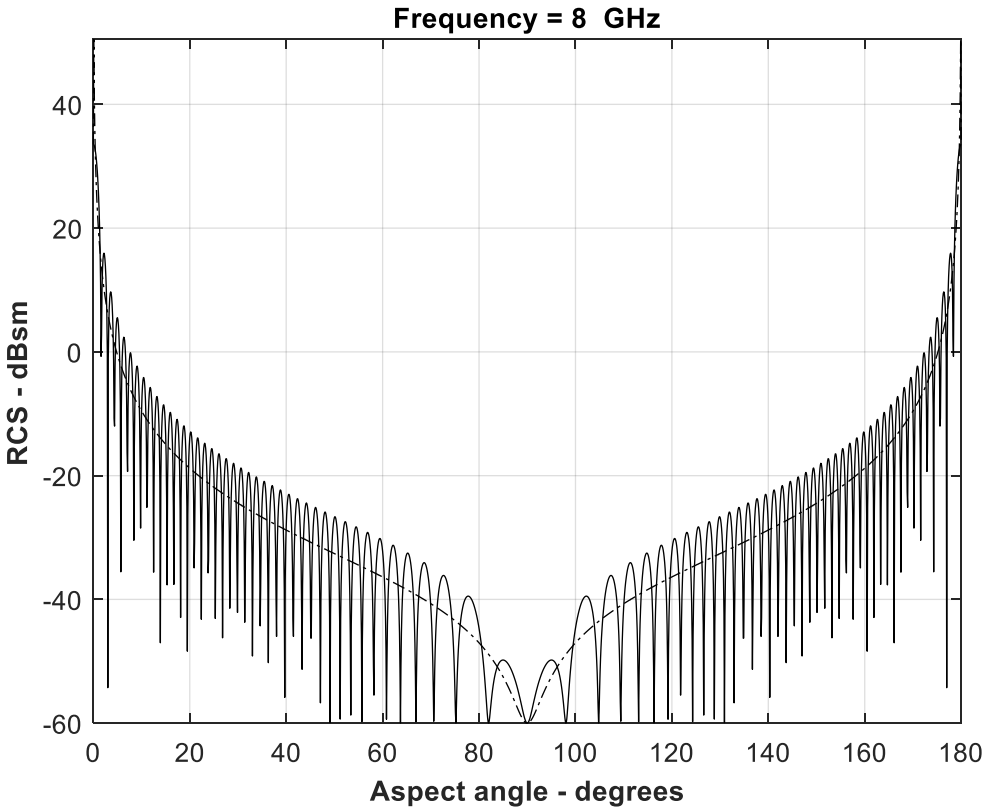

Figure 3.8: Backscattered RCS of circular flat plate

In the above figure the solid heavily curved line corresponds to Eq. 3.17 and the dashed line corresponds to Eq. 3.16.

3.7.3 Circular Cylinder

In the case of calculating the RCS of a cylinder having circular surface which is referred to as a circular cylinder. For circular cylinder of radius r and height h, the backscattered RCS is given as

$$\sigma = \frac{2\pi r h^2}{\lambda} \theta = 0° \tag{3.18}$$

$$\sigma = \frac{\lambda r sin\theta}{8\pi (cos\theta)^2} \theta \neq 0° \tag{3.19}$$

The RCS plot corresponding to the equations (3.18, 3.19) using MATLAB is shown in Figure 3.9. The figure indicates that RCS depends on aspect angle and the broadside speculum occurs at aspect angle of $\frac{\pi}{2}$.

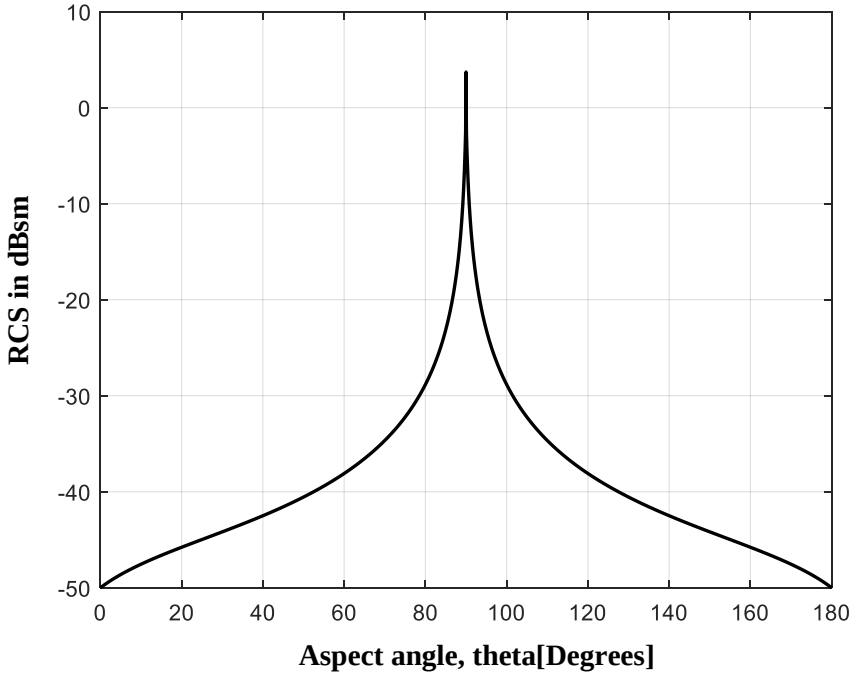

Figure 3.9: Backscattered RCS of a circular cylinder

In the case of a cylinder it is found that the RCS variation as a function of aspect angle is quite equally distributed for values calculated at same distances on both side of 90°. So it can be stated that the normal incidence or maximum RCS occurs at 90° aspect angle which is quite high and decreases on both sides equally.

3.8 RCS of Complex Objects

At this part of the work, we have considered a number of stationary targets for our discussion. This kind of backscattered RCS is often called static RCS. In most practical radar systems there is relative motion between the radar and an observed target. It means, the observed target is motional related to radar. The RCS of complex objects such as aircrafts, missiles and fabricated structures varies significantly with viewing aspect and frequency. This observed RCS is referred to as the radar dynamic cross section. On this basis, we have taken these two parameters on our target object and measure the RCS of this.

The variability in the complex RCS results from the multiple individual scatterers that constitute the object. Each individual scatterer of a complex target produces an echo signal characterized by amplitude and a phase. Dynamic RCS may fluctuate which is called scintillation [34]. A complex target RCS is normally simulated by coherently combining

the cross sections of the simple multiple shapes that make that target. In general, a complex target RCS can be modeled as a group of individual scattering centers distributed over the target object.

Complex targets that can be modeled by many equal scattering centers are often called swirling 1 or 2 targets. Alternatively, targets that have one dominant scattering center and many other smaller scattering centers are known as swirling 3 or 4 targets.

As an example, consider a circular cylinder with two perfectly conducting circular flat plates on both ends. Assume linear polarization and let H = 1 m and r = 0.125 m. The backscattered RCS for this object versus aspect angle is known in Figure 3.10.

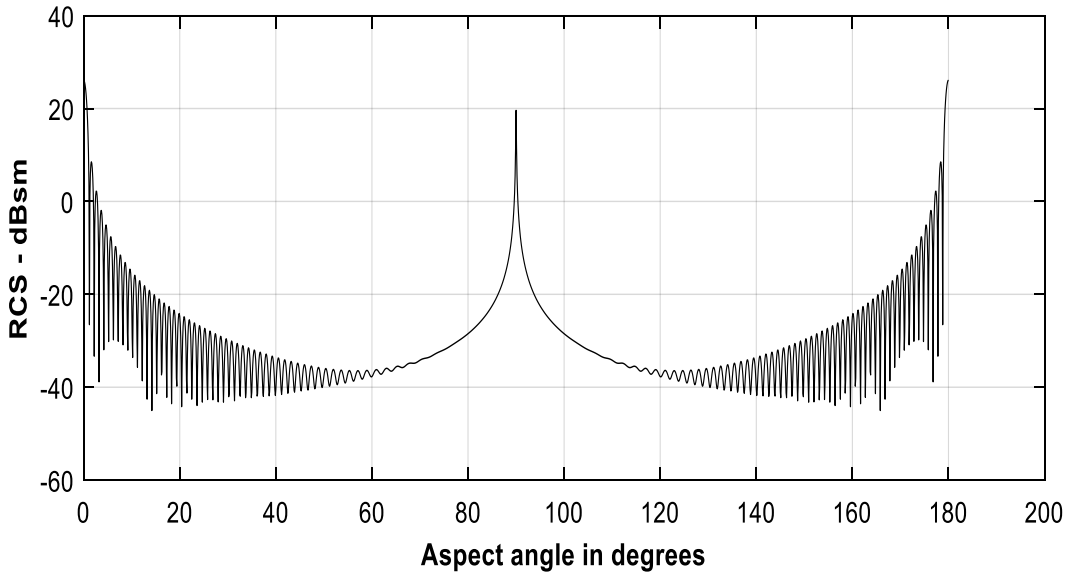

Figure 3.10: Backscattered RCS of a cylinder with flat plates [5]

From the simulation it was revealed that at aspect angles close to $0°$ and $180°$, RCS is mainly dominated by the circular plate, while at aspect angles close to normal incidence, the RCS is specifically dependent on the cylinder broadside specular return.

Chapter 4

SIMULATION AND OVERVIEW

4.1 RCS Measurement

Concept of electromagnetic energy scattering by any object is very important in the understanding of RCS of targets. RCS reduction is necessary to analyze the reflection of conducting, dielectric and magnetic surfaces. Within this context, RCS analysis of targets with simple shapes is fundamental to support the understanding of RCS patterns of targets with complex configuration. It is difficult theoretically to estimate RCS of complex targets as it is impossible to include all practical phenomena into consideration. The evolution of electromagnetic scattering of target can be carried out experimentally or by computer simulation.

4.2 RCS Measurement Methods

The methods of RCS measurement through experiment are driven by size of target, frequency of measurement etc. Based on these requirements, measurement can be done in two ways:

- Far-field outdoor range
- Anechoic Chamber compact range

4.2.1 Far-field Outdoor Range

The RCS measurements need a transmitter, a receiver, and a positioning system for the target under test. Transmitting antenna should generate a plane wave at the target. The target should create far-field at the receiving antenna. This is possible in an open space; however, the locations of transmitter, receiver and target are to be fixed such that there are no reflections from the near environment and the ground.

Actually, it is difficult to stop reflections from the ground. There are two possibilities of implementation of the outdoor range in context to ground reflection:

- Ground plane reflection is used in the measurements,
- Ground plane reflections are defeated using fences, berms or absorbers.

The first approach of mounting a sizable target on a range and isolating it from the effects of the ground was recognized early on as nearly impossible to achieve. It was realized that the most effective way of dealing with ground reflections was to exploit the ground surface as a participant in the process of illumination using absorbers [13].

The parameters that affect the performance of testing are transmitter height (H_{tx}), target height from ground (H_t), operational frequency, range separation distance (R). The measurement requirement is to position the target whose reflectivity characteristics are to be evaluated on an elevated platform termed as pylon at target location.

To mount and rotate targets when their RCS is being measured, special pylons have been designed which have very low backscatter when viewed the radar. Typically, the cross sectional shape of a pylon is ogival (two intersecting circles) and the pylon body tapers from its base to the top where a modest seized rotator attaches. The rotator is capable of rotating a target through 360 degrees in azimuth and through perhaps 45 degrees in elevation.

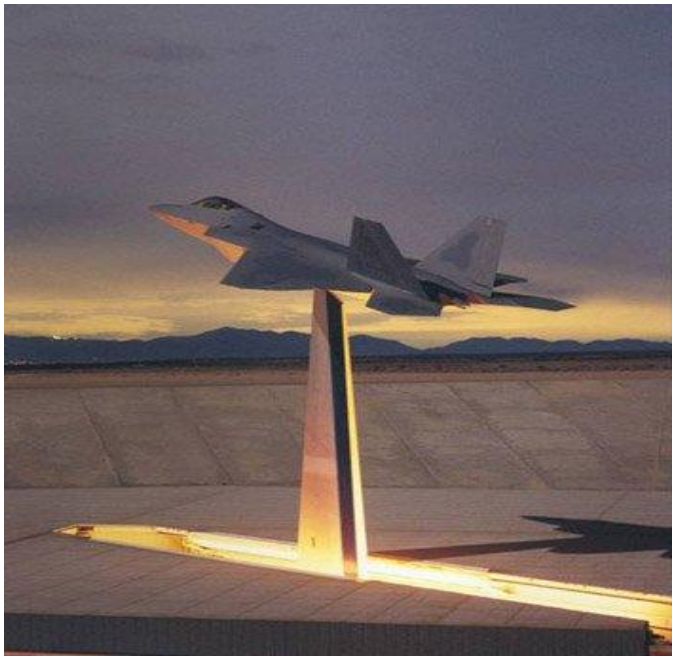

Figure 4.1: Outdoor RCS measurement of a aircraft, fixing on pylon

Far-field distances often require 5000 to 10000 feet or range length with a controlled ground surface to control reflections [13].

4.2.2 Anechoic Chamber Compact Range

A compact range is a device for creating plane-wave illumination in a laboratory at microwave frequencies. The governing equation for operation of a point source compact range for RCS measurement is [14]

$$\frac{P_{scat}^{Rcv}}{P_0^{Xmt}} = \frac{1}{(4\pi)^3}\left(\frac{\sigma}{\lambda^2}\right)\left(\frac{\lambda}{R_o}\right)^4 G_F^2 \tag{4.1}$$

Where,

P_{scat}^{Rcv} = Power scattered by target and received by radar

P_0^{Xmt} = Power from the transmitter

λ = Wavelength of radiation

R_o = Distance from focus to reflector

G_F = Gain of feed

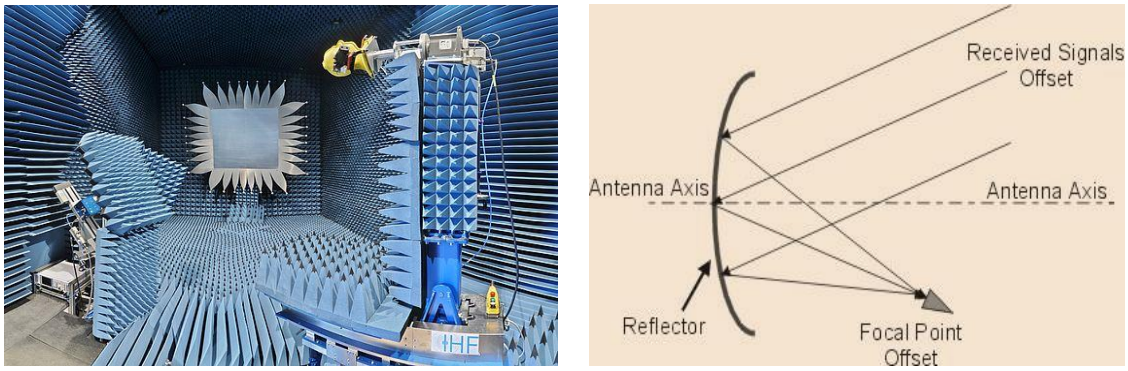

(a) (b)

Figure 4.2: Indoor compact range measurement using point source and reflector. (a) Real time anechoic chamber, (b) Ray diagram of measurement process.

Compact range uses the reflective properties of a paraboloidal reflector to correct the phase curvature of electromagnetic wave radiated from a small antenna at the focal point of the reflector. The reflected wave is collimated and the phase curvature is substantially corrected to simulate far-field conditions within a compact range. The compact range requires a special anechoic chamber having high quality RAM on the end wall. The collimating effect of the reflector deemphasizes the effect of the chamber walls, floor and ceiling allowing the use of less stringent RAM.

4.3 Target Model

A radar system relies on target reflection or scattering to detect and identify targets. The more strongly a target reflects, the greater the returned echo at the radar receiver, resulting in a higher signal-to-noise ratio (SNR) and likelier detection. In radar systems, the amount of energy reflected from a target is determined by the radar cross section (RCS), defined as

$$\sigma = \lim_{R\to\infty} 4\pi R^2 \frac{|E_s|^2}{|E_i|^2} \tag{4.2}$$

where σ represents the RCS, R is the distance between the radar and the target, E_s is the field strength of the signal reflected from the target, and E_i is the field strength of the signal incident on the target. In general, targets scatter energy in all directions and the RCS is a function of the incident angle, the scattering angle, and the signal frequency. RCS depends on the shape of the target and the materials from which it is constructed. Common units used for RCS include square meters or dBsm.

The simplest target model is an isotropic scatterer. An example of an isotropic scatterer is a metallic sphere of uniform density. In this case, the reflected energy is independent of the incident angle. An isotropic scatterer can often serve as a first order approximation of a more complex point target that is distant from the radar. For example, a pedestrian can be approximated by an isotropic scatterer with a 1 square meter RCS.

For targets with more complex shapes, reflections can no longer be considered the same across all directions. The RCS varies with the incident angles (also known as aspect angles). Aspect-dependent RCS patterns can be measured or modeled just as you would

antenna radiation patterns. The result of such measurements or models is a table of RCS values as a function of azimuth and elevation angles in the target's local coordinate system.

4.3.1 Stealth Technology

Stealth aircraft are designed to avoid detection using a variety of technologies that reduce reflection/emission of radar, infrared, visible light, radio frequency spectrum and audio, collectively known as stealth technology. While no aircraft is totally invisible to radar, stealth aircraft make it more difficult for conventional radar to detect or track the aircraft effectively, increasing the odds of an aircraft successfully avoiding detection by enemy radar and/or avoiding being successfully targeted by radar guided weapons. Stealth is the combination of passive low observable (LO) features and active emitters such as low-probability-of-intercept radars, radios and laser designators. The idea behind stealth aircraft was theorized by a Soviet mathematician, who in the 1960s found that the strength of a radar return wasn't related to the object's size, but instead related to the edge configuration of the object [14].

4.3.2 F-117A Nighthawk Stealth Fighter Jet

For the analytic simulation purposes we chose the F-117A Nighthawk Stealth Fighter, which is the practically world’s first operational stealth aircraft [15].

Figure 4.3: A flying F-117A Nighthawk

It was the lowest observable platform in the history of aeronautics with very low radar cross section which makes it a true stealth aircraft. A diamond shaped aerodynamic design which is very effective to fool most of the radars.

The US stealth project began in 1975, and the first two prototypes, code name "Have Blue", were built using T-38 jet engines, F-16 fly-by-wire systems, A-10 landing gear, and C-130 environmental systems. The F-117 was made entirely of flat surfaces which were initially based and flown at the Tonopah Test Range, the same facility used to test fly acquired Soviet aircraft. It used a quadruple-redundant fly-by-wire system to keep the inherently unstable jet airborne. The F-117 holds the record for longest non-stop single-seat fighter flight, when it was flown from Holloman AFB in New Mexico to Kuwait, with aerial refueling. 64 production F-117s were built and flown over the course of 27 years. The F-117 was retired in 2008, but it still lives on as the world's first production stealth aircraft [16].

4.4 COMSOL Multiphysics

COMSOL Multiphysics (the name is meant to be an acronym of COMmon SOLution) is a cross-platform finite element analysis, solver and multiphysics simulation software. COMSOL creates a simulation environment facility for all the steps of the modeling process- defining the model geometry, meshing, specifying the physics of simulation, solving and lastly visualizing the results [17]. It allows conventional physics-based user interfaces and coupled systems of partial differential equations (PDEs). COMSOL provides an IDE and unified workflow for electrical, mechanical, fluid, and chemical applications. An Application Programming Interface (API) for Java and Live Link for MATLAB may be used to control the software externally, and the same API is also used via the Method Editor.

COMSOL contains an App Builder which can be used to develop independent domain-specific apps with custom user-interface. Users may use drag-and-drop tools (Form Editor) or programming (Method Editor). Specific features may be included from the model or new features may be introduced through programming. It also contains a Physics Builder to create custom physics-interfaces accessible from the COMSOL Desktop with the same look-and-feel as the built-in physics interfaces [18].

4.4.1 2D Target Model Design

The F-117 Nighthawk is first designed as a 2D CAD model in SOLIDWORKS 2015. Then in COMSOL Multiphysics the CAD model is imported. Finalized geometry has 95 domains, 742 boundaries, and 664 vertices. Formed union of 2 solid objects. Mesh consists of 7194 domain elements and 644 boundary elements. Number of degrees of freedom solved for: 51514. Practically, F – 117 was designed with a number of almost flat facets constructed with aluminum. For convenience of calculation and accuracy, we fragmented the target object into 178 facet like areas. All the facets are not equal in dimension and so the reflected radar signal from these facets would definitely vary from each other.

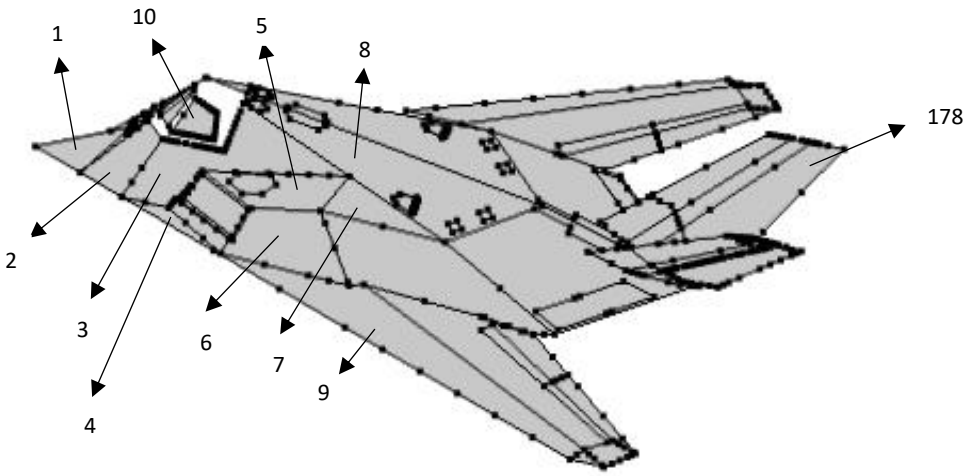

Figure 4.4: 2D CAD Model of F-117A

In Figure 4.4, the 2D model was fragmented through five major categories. Wingspan, Upper Surface, Tail (each of them was considered for both right and left side of the target), Lower surface, Window. Window is also considered as metallic surface to the radar as there is special coating on the cockpit canopy. These 178 fragmental areas are the base of RCS measurement. Lockheed Martins. Co. specifies F-117 construction with four elevons set up on inboard and outboard with the trailing edge of the wings. The V-shaped tail acts as control surface. The stealth target is constructed of aluminum and for the engine and exhaust system it is sheathed with titanium [19].

4.5 F-117A RCS Simulation and Result

4.5.1 Near Field Simulation

Near field computation consists of a virtual radial shape anechoic chamber where the target object is placed at the center and from different angle of the circle radar radiation is introduced. The circle represents a perfect electric conductor (PEC) which avoids unwanted outside radiation from prevailing [20].

4.5.2 Perfectly Matched Layer

The F-117A CAD model as target object and the incident field interaction is computed through COMSOL Multiphysics interface. The object is very much complex and it meets the electromagnetic waves from a distant radar transmitter. The transmitter is set at a distance so that the field can be thought of as a plane wave. A perfect electric conductor (PEC) is set at 15 m radius. PEC allows us to create a virtual anechoic chamber of a compact range which is a device for creating plane-wave illumination in a laboratory at microwave frequencies. Within the circle of PEC, a perfectly matched layer (PML) is created at a radius difference of 3 m which is illustrated in Figure 4.5.

$$n \times E = 0 \tag{4.3}$$

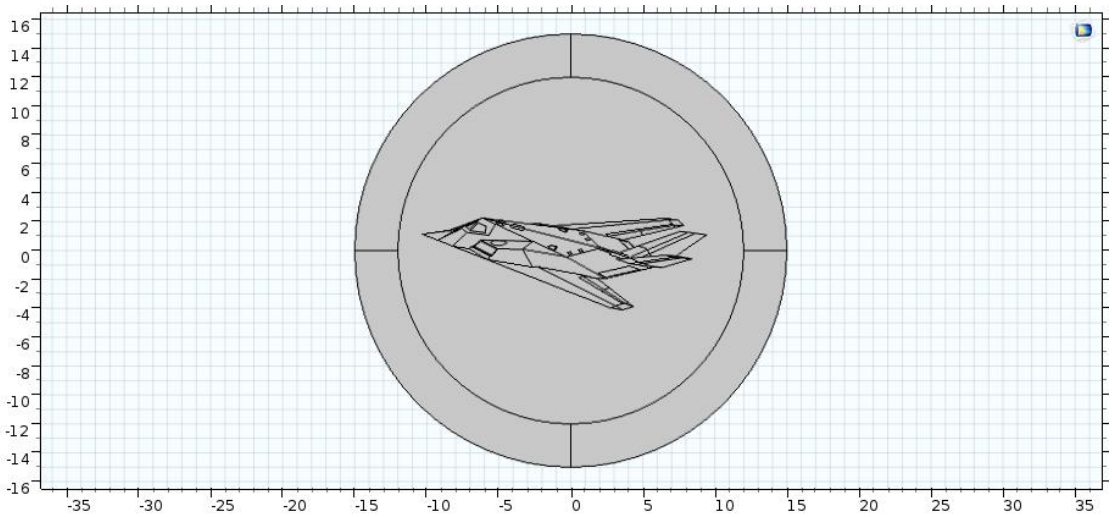

Figure 4.5: Model geometry of F-117

In the Figure 4.5, the inner circle represents air field and the outer circle is perfectly matched layer that minimizes the unphysical reflections of scattered wave. According to COMSOL Multiphysics software, the inner circle needs to surround the object completely

to minimize the CPU time and memory usage. The outer circle also needs to be proportionate according to PML's meshing need [21].

$$E_b = \exp(\mathrm{j}k_o(x\cos\varphi + y\sin\varphi)) \tag{4.4}$$

Where,

E_b = Backscattered electric field

j = An imaginary unit

k_0 = Wave number

φ = Angle of incidence.

4.5.3 Impedance Boundary Condition

The F-117A target model point boundaries are selected for impedance boundary condition. The use of an impedance boundary condition assumes that the skin depth in the material is much less than the material thickness. At 200 MHz, the skin depth in Aluminum is of the order of microns, so it is safe to say this is the case. At absolute pressure of 1 atm, optimum temperature of experiment is considered 293.15 K, the impedance boundary condition is defined as [22]

$$\sqrt{\frac{\mu_o\mu_r}{\epsilon_o\epsilon_r - j\sigma l\omega}} \times n \times H + E - (n.E)n = (n.E_s)n - E_s \tag{4.5}$$

Where,

μ_o = Permeability of free space

μ_r = Relative permeability

ϵ_o = Permittivity of free space

ϵ_r = Relative permittivity

σ = Radar cross section

H = Magnetic field strength

E = Electric field strength

ω = Angular frequency

E_s = Incident electric field strength

n = Number of waves

4.5.4 Mesh Analysis

For this very much complex geometry, Comsol performs a mesh analysis in its mesh building function including the PML. The prominent points show that RCS signature at the edges in simulated output of the mesh graph which is illustrated in Figure 4.6.

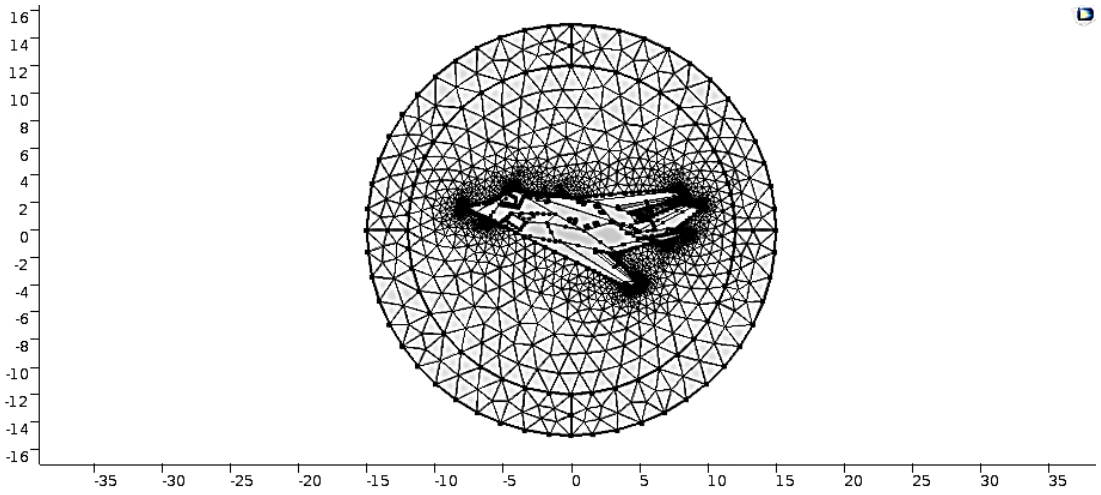

Figure 4.6: Mesh analysis of target.

Solving the relative field with time harmonic wave equation, we get the measured total field that indicates how detectable the target is with radar. We have assumed that the target is static (or equivalently, that the Doppler shift has been precisely measured and compensated) [23].

4.5.5 Aspect Angle Variation

In engineering, aspect angle is the angle formed between the longitudinal axis of a projectile in flight and the axis of a radar beam. Figure 4.7 illustrates the idea of aspect angle

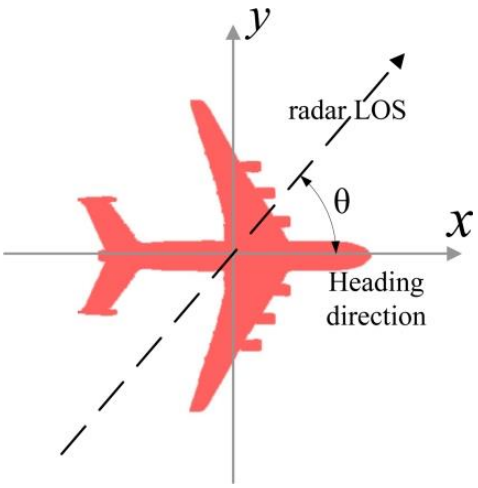

Figure 4.7: Aspect angle (θ)

The aspect angle θ is defined as the angle between the major axis of the target (heading direction) and the radar LOS.

Now a parametric sweep is initiated based on the aspect angle. The sweeping is done for full range of incidence angles from 0 to 359 degree with 1 degree step. For the target object, various aspect angles were measured and some of them are as follows-

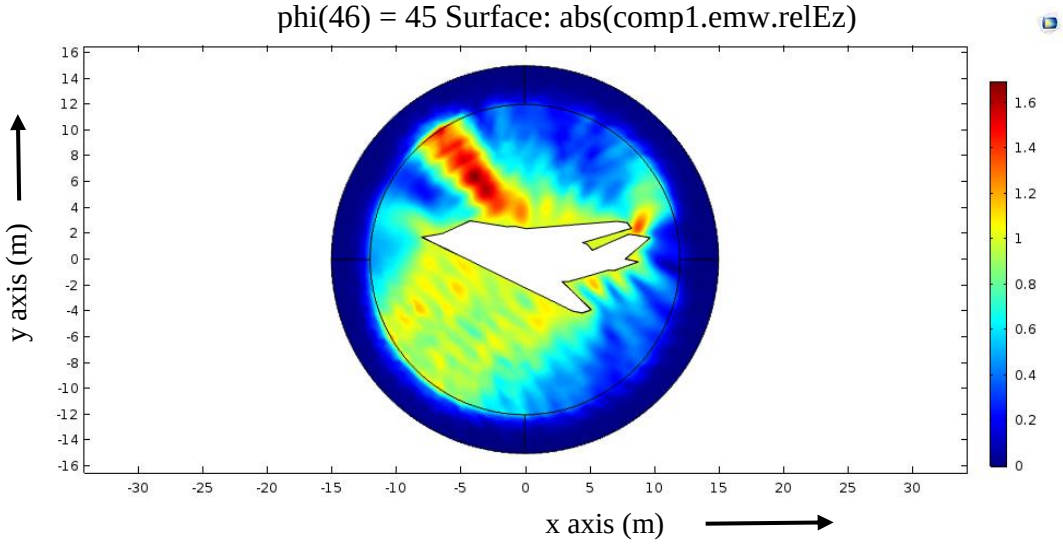

(a) Aspect angle 45°

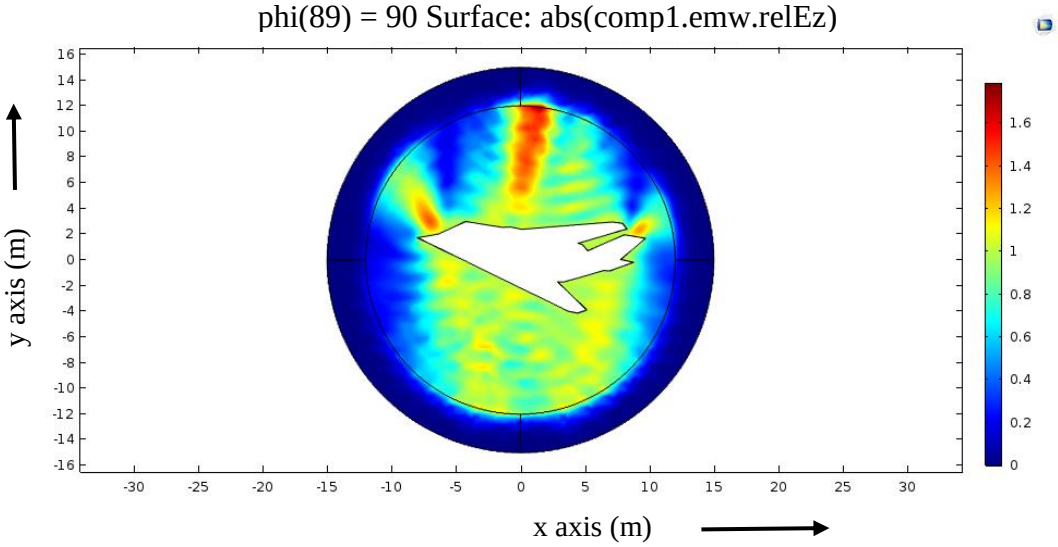

(b) Aspect angle 90°

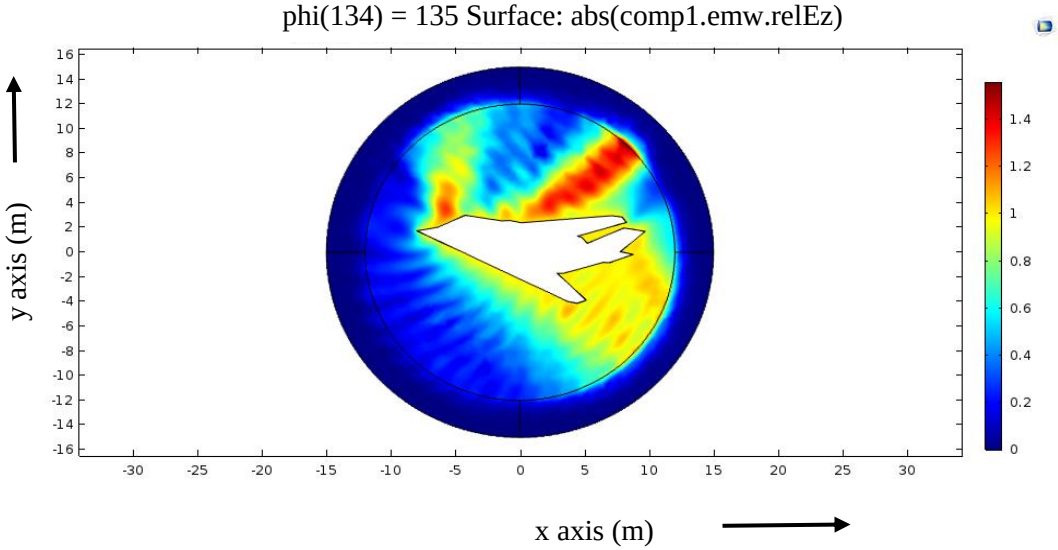

(c) Aspect angle 135°

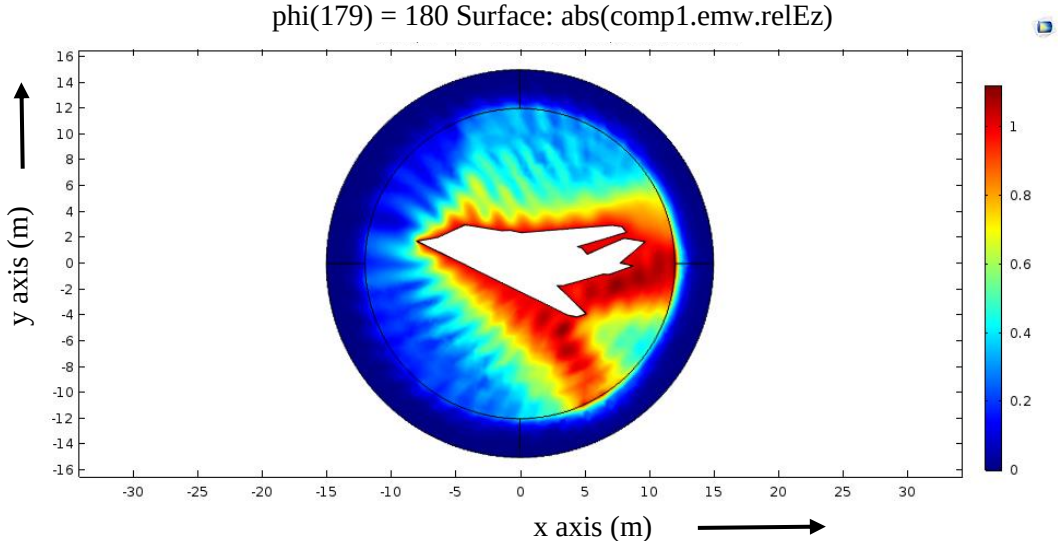

(d) Aspect angle 180°

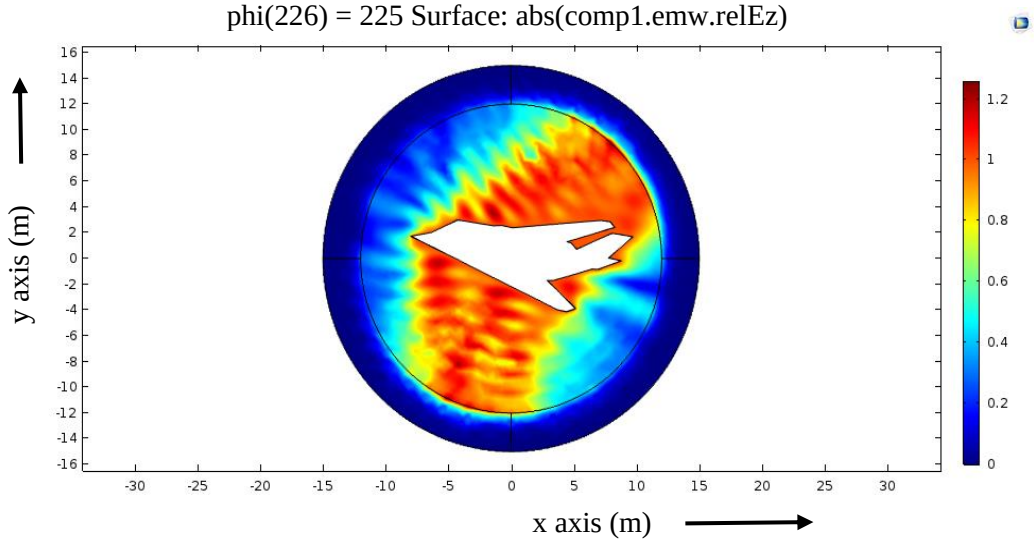

(e) Aspect angle 225°

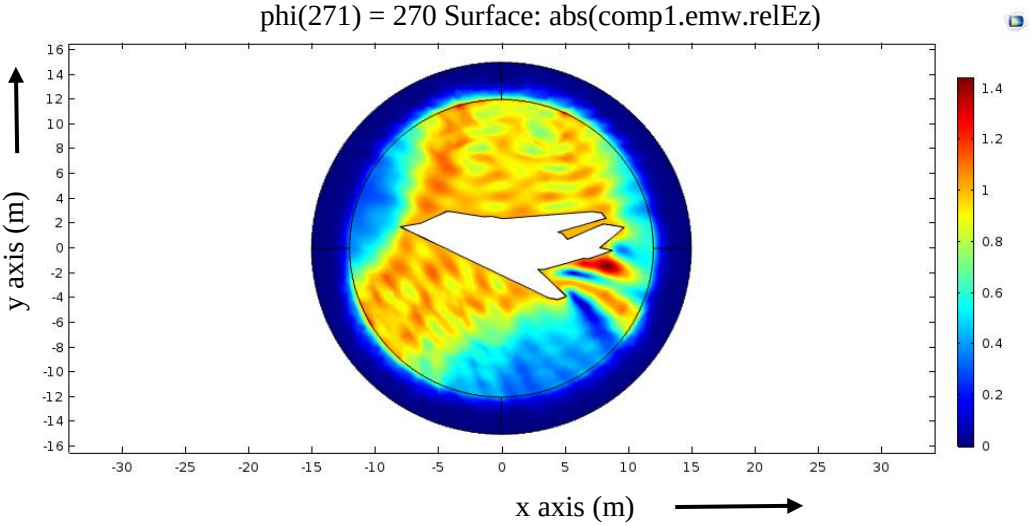

(f) Aspect angle 270°

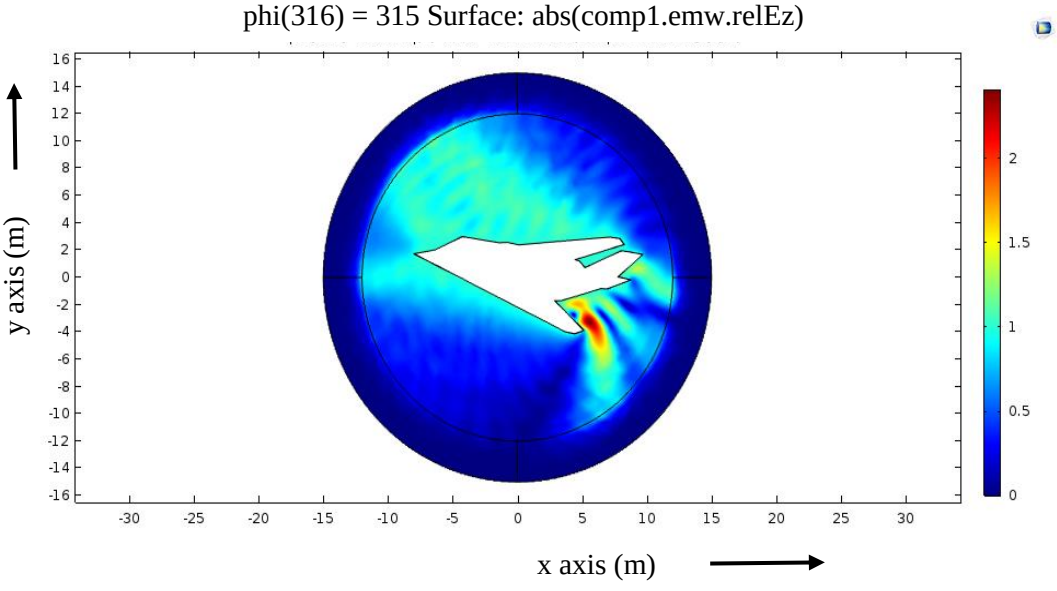

(g) Aspect angle 315°

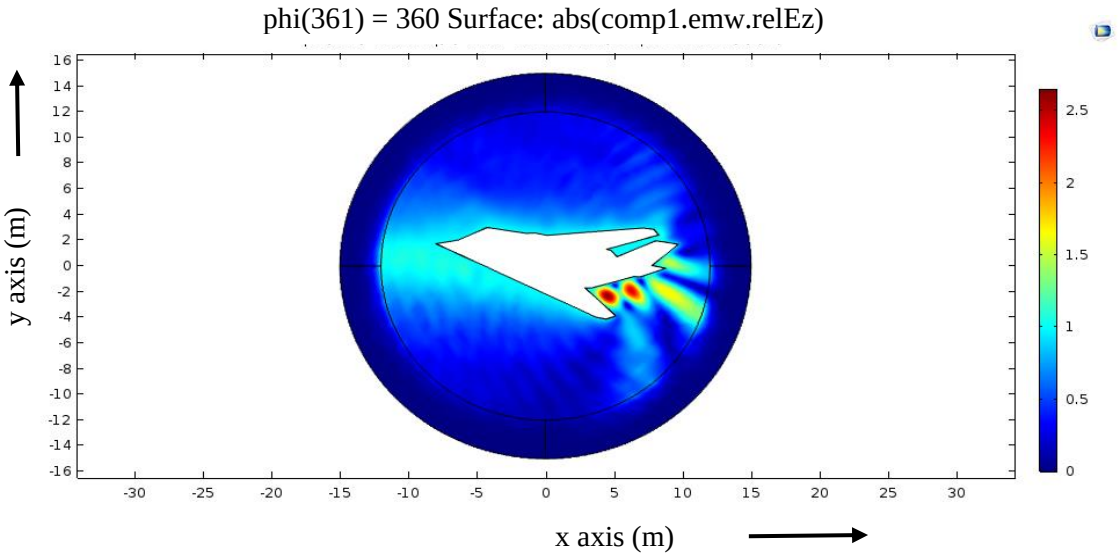

(h) Aspect angle 360°

Figure 4.8: Absolute surface electric field normal at z direction at different aspect angles.

4.5.6 Frequency Variation

Another parameter is varied for the F-117A during simulation and that is radar incident signal frequency. For specific purposes, S band (2-4 GHz) and X band (8-12 GHz) band are chosen for our experiment. S band is used for moderate range surveillance, Terminal air traffic control, long-range weather, marine radar etc. X band is used for missile guidance, marine radar, weather, medium-resolution mapping and ground surveillance. In the United States the narrow range 10.525 GHz±25 MHz is used for airport radar. Named X band because the frequency was a secret during World War II .

Frequency was swept in the setup configuration for F-117A and the polar plot graph is plotted. The graph is plotted in the manner of RCS vs aspect angle at a fixed frequency. The inner circles indicate the RCS in dBsm and the outer circle is considered for the aspect angle measurement.

For S band,

For S band the polar plot graphs are as follows -

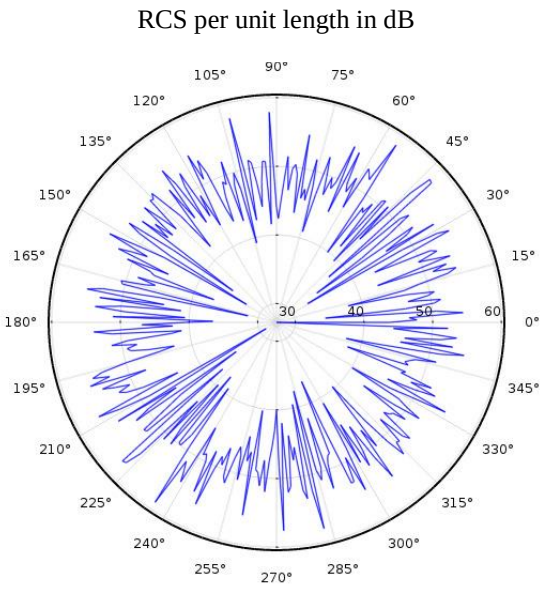

(a) RCS at S band (Lower range – 2 GHz)

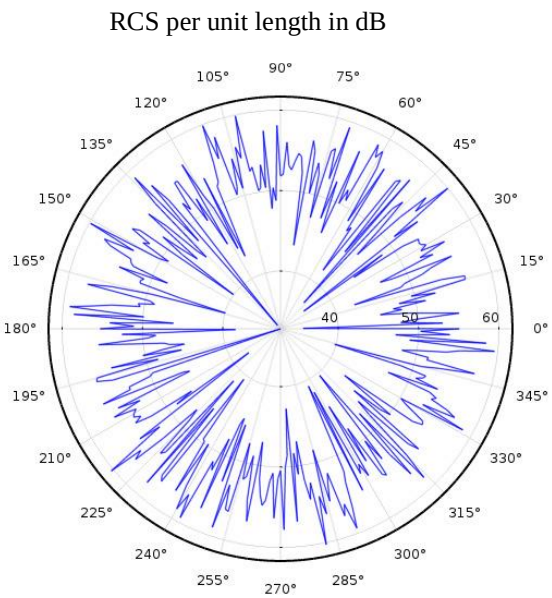

(b) RCS at S band (Upper range – 4 GHz)

Figure 4.9: Polar plot graph for S band

It has been seen from the polar plot point graph that, at different angles of incidence, RCS significantly vary. In between 2 ~ 4 GHz, multiple frequencies were considered at an

interval of 400 MHz. Those results are plotted in the same graph and thus the highest value along with nearby values for that specific frequency are pointed out in Figure 4.9.

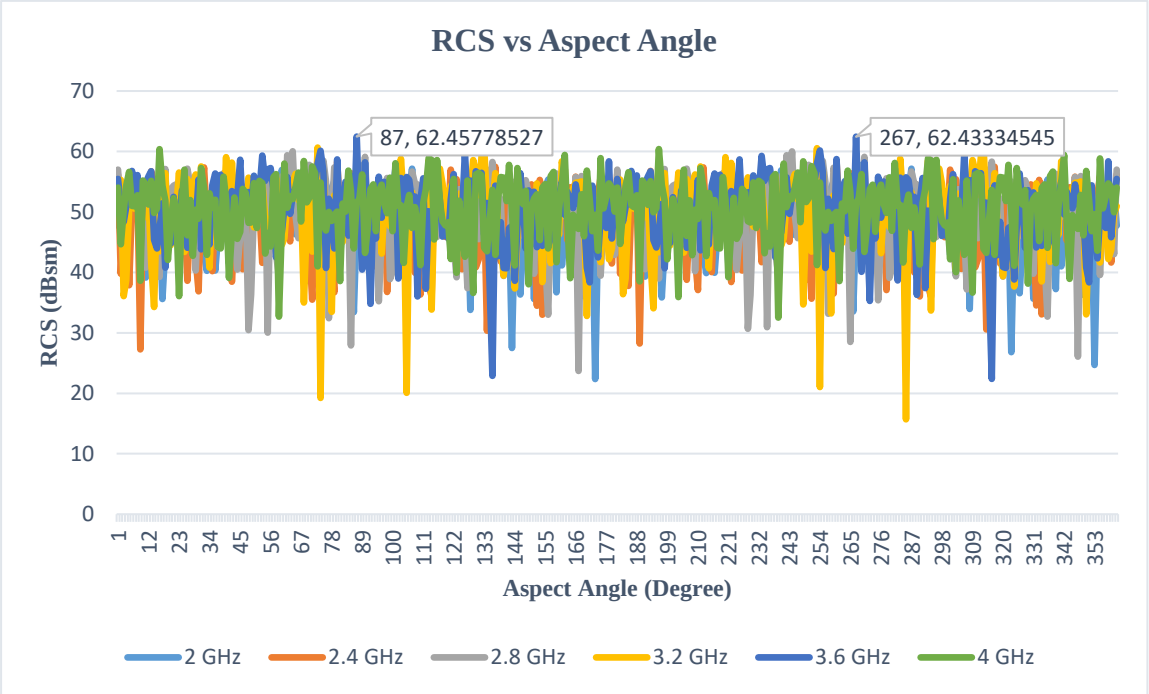

Figure 4.10: RCS dependency on aspect angle at S band

From the above Figure 4.10, it is notable that if the radar frequency is set at 3.6 GHz (for S band) and aspect angle is set at 87 degree or 267 degree radar will show maximum RCS (here, 62.45778527 or 62.43334545 respectively) for a given complex object (F-117A).

Focusing on previous simulation results we selected the parameters at its best outcome and simulated again. This shows the best possible RCS output for our target object which is shown in Figure 4.11.

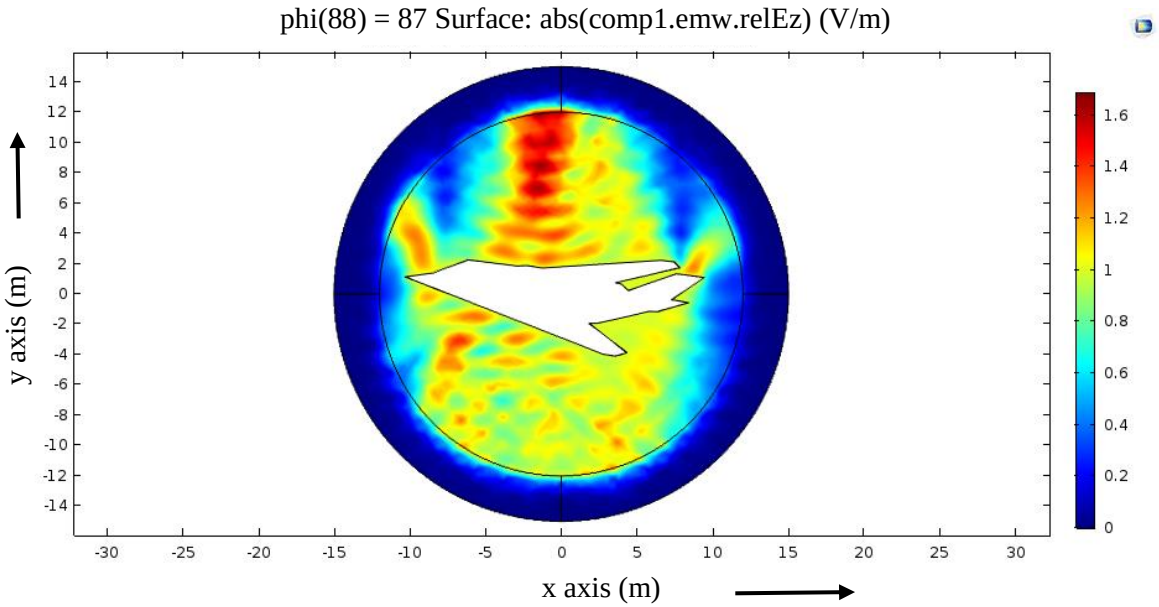

(a)

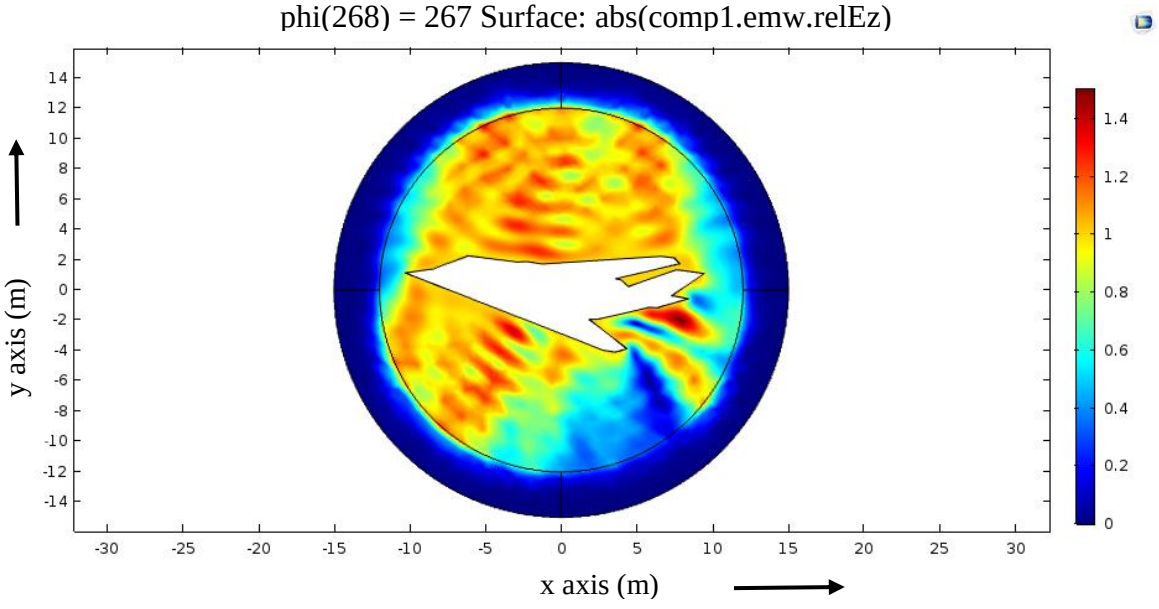

(b)

Figure 4.11: At 3.6 GHz the best RCS output at (a) 87°, (b) 267°

For X band,

Following the same process for X band yields the following results.

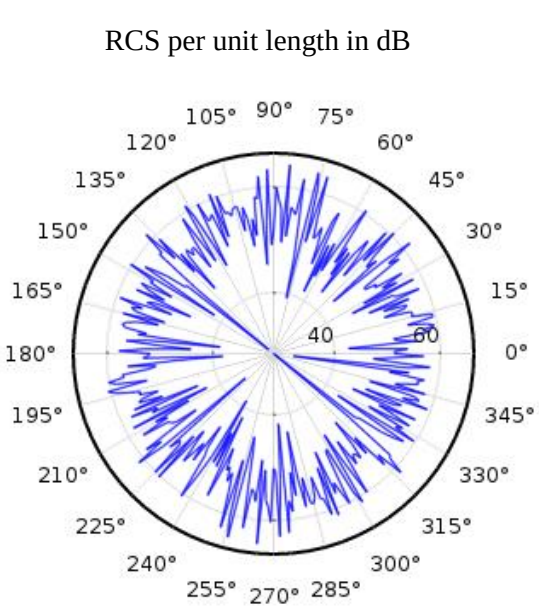

(a) RCS at X band (Lower range – 8 GHz)

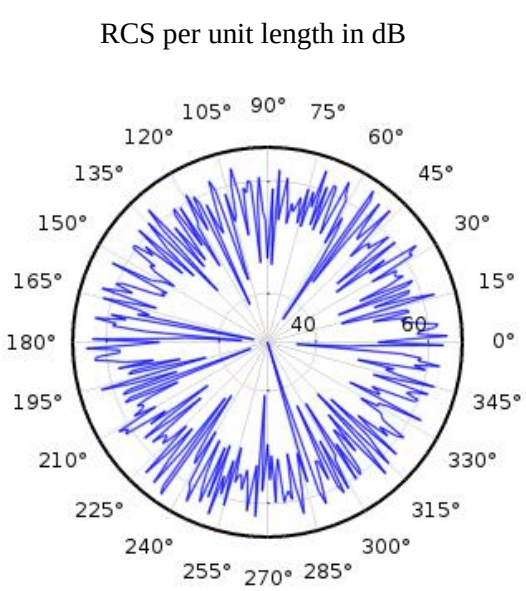

(b) RCS at X band (Upper range – 12 GHz)

Figure 4.12: Polar plot graph for X band

Similarly, plotting the frequencies at an interval of 0.4 GHz we get the generalized relation of RCS and aspect angle for that particular frequency as graphical data.

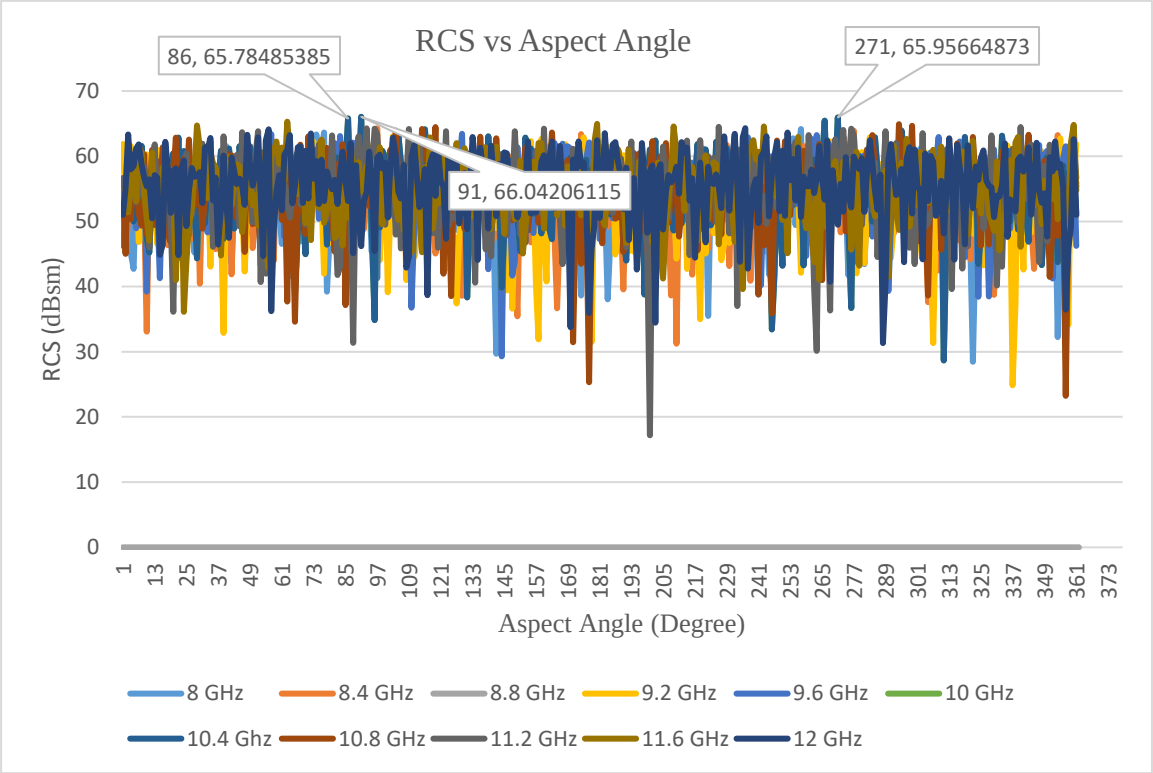

Figure 4.13: RCS dependency on aspect angle at X band

From the above figure it is notable that if the radar frequency is set at 10.4 GHz (for X band) and aspect angle is set at 86, 91 or 271 degree radar will show maximum RCS (here, 65.7848585, 66.04206115 and 65.95664873 respectively) for a given complex object (F-117A).

Focusing on previous simulation results we selected the parameters at its best outcome and simulated again. This shows the best possible RCS output for our target object which is shown in Figure 4.14.

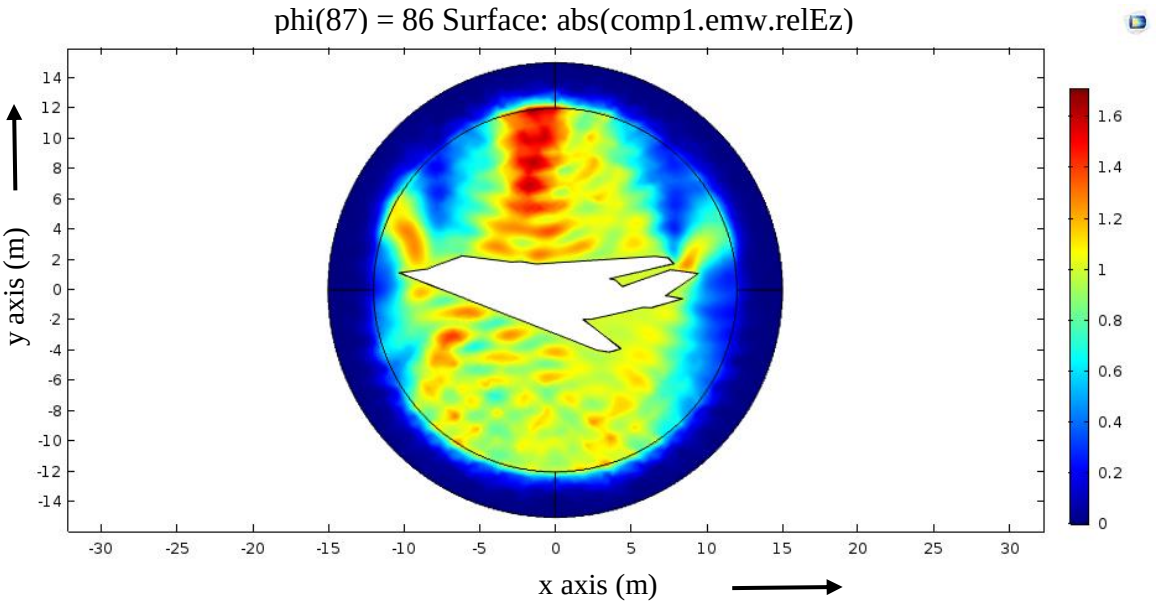

(a) Aspect angle 86°

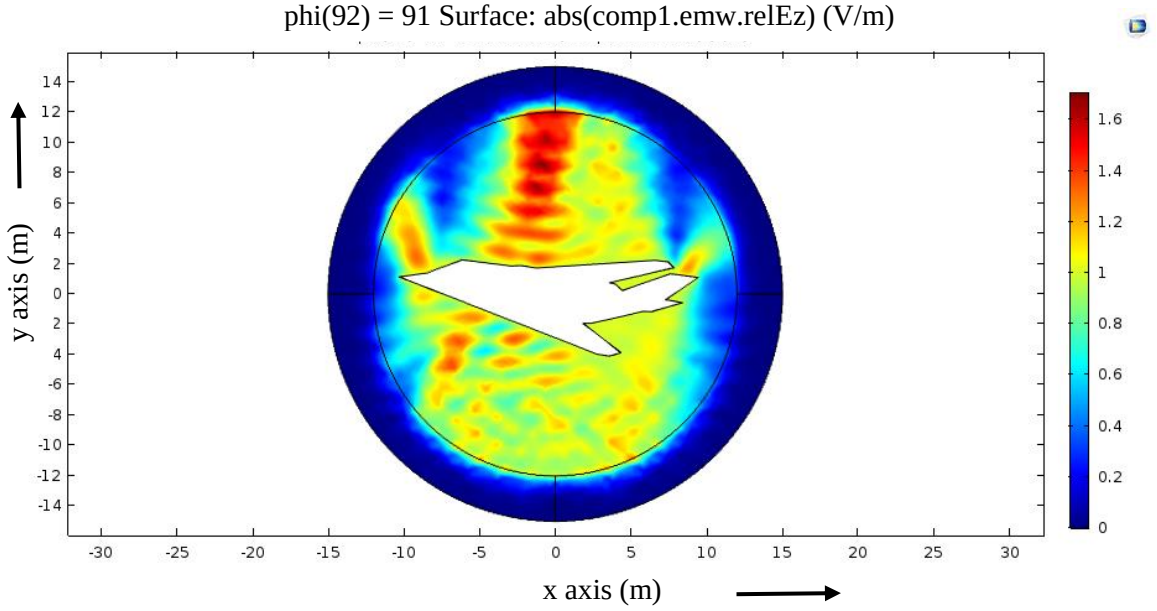

(b) Aspect angle 91°

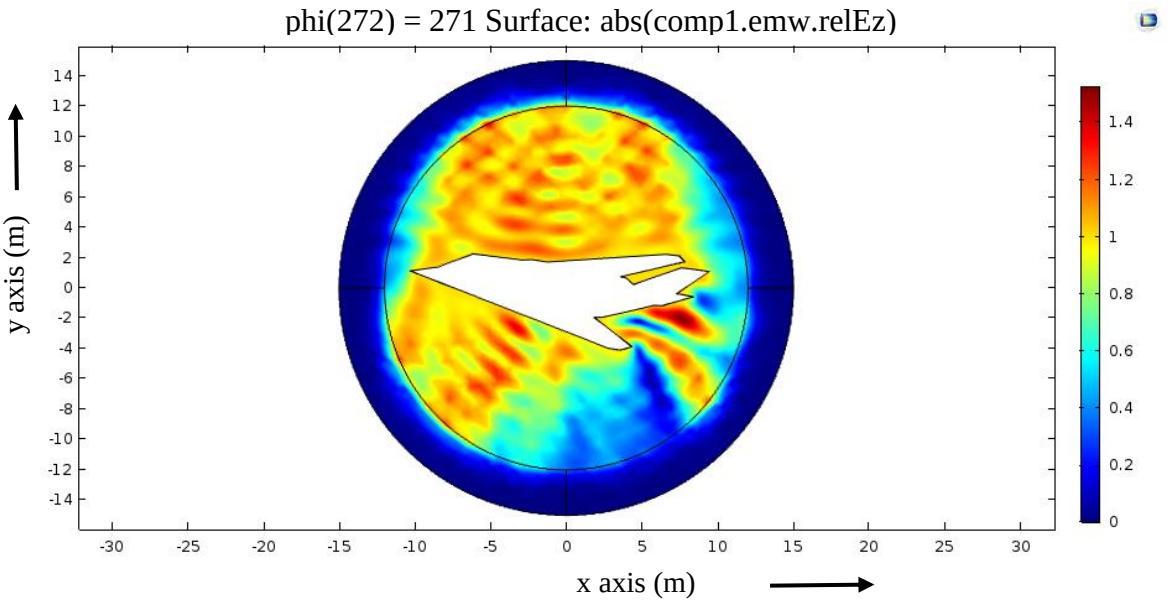

(c) Aspect angle 271°

Figure 4.14: At 10.4 GHz the best RCS output at (a) 86°, (b) 91°, (c) 271°

The side colorful bar represents the color legend. It shows how the scattering relative electric field is changing based on the target object.

4.5.7 Far Field Simulation

In order to keep the required computational resources reasonable, a small model region of space around the antenna is created. Then this small simulation domain with an absorbing boundary is truncated, such as a perfectly matched layer (PML), which absorbs the outgoing radiation. Since this will solve for the complex electric field everywhere in our simulation domain, we will refer to this as a *Full-Wave* simulation [24]. Then information is extracted about the antenna's emission pattern using a *Far-Field Domain* node, which performs a near-to-far-field transformation [25].

In this thesis work, that small circle of 15 m radius is our model region surrounding by PML and in the same way normalized far field strength is measured in dB. For our best aspect angles through simulation (87°, 91°), the far field calculation is done.

For 87°

For 87° aspect angle the far field surface and calculation depending on angle of incidence has been carried out and shown in Figure 4.15.

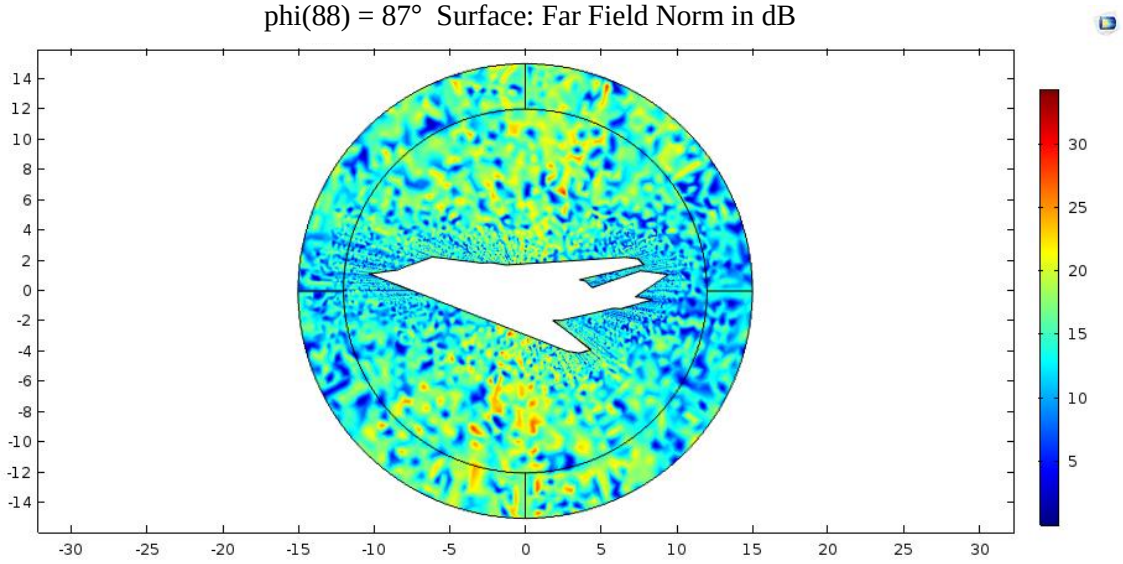

(a) Normalized Far Field surface at φ =87°

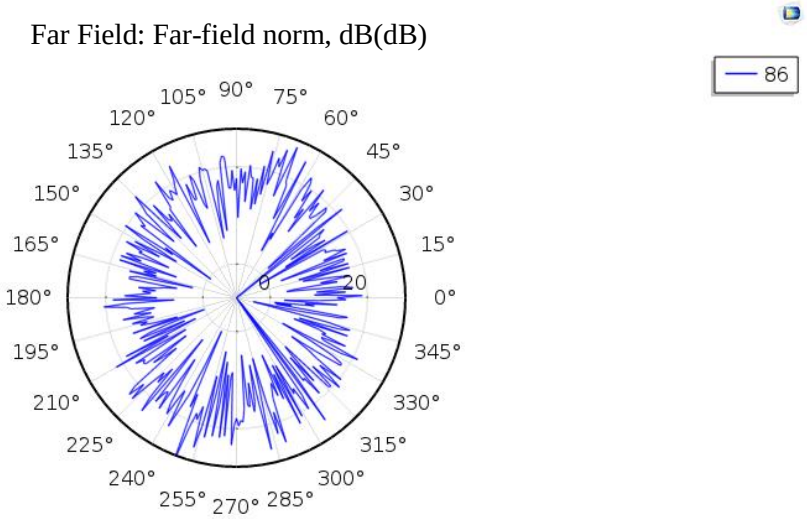

(b) Polar plot point graph with Far Field distribution along r-axis

Figure 4.15: Far Field Simulation for 87°

Far Field calculation leads us to the far field domain analysis. If any target shape like F-117A approaches to any specific radar far field, it will show the normalized far field characteristics around 87° of angle of incidence like Figure 4.15(a).

Figure 4.15(b) illustrates the far field distribution from the target object when the radiation is initiated from 87°. Along the r-axis, the normalized far field is measured. On an average, 14.26095083 dBsm is recorded as our result.

For 91°

The same procedure has been carried out for another best possible aspect angle 91° and illustrated in Figure 4.16.

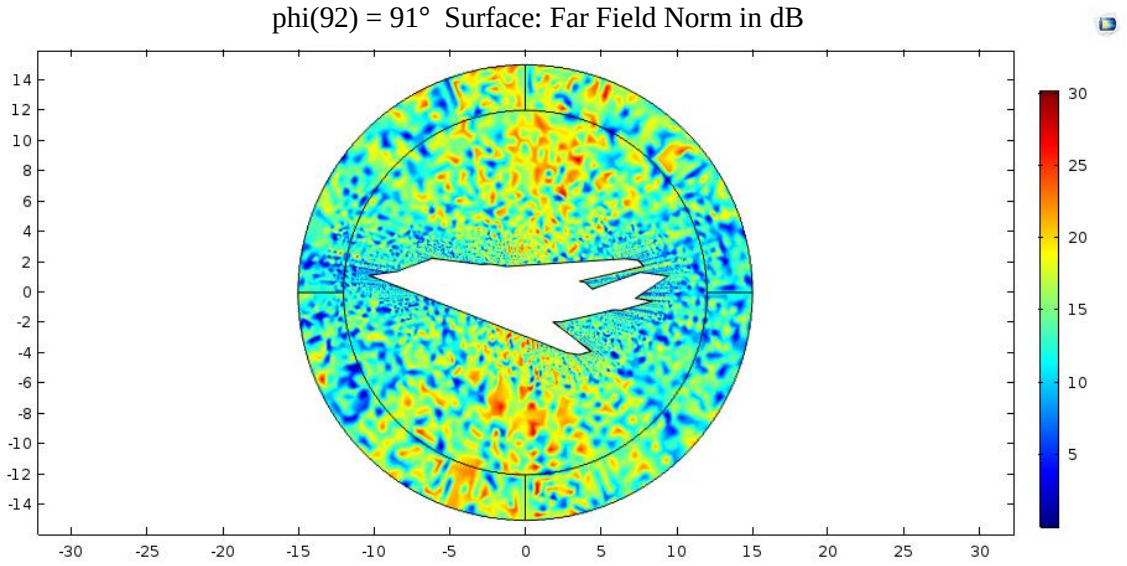

(a) Normalized Far Field surface at φ =91°

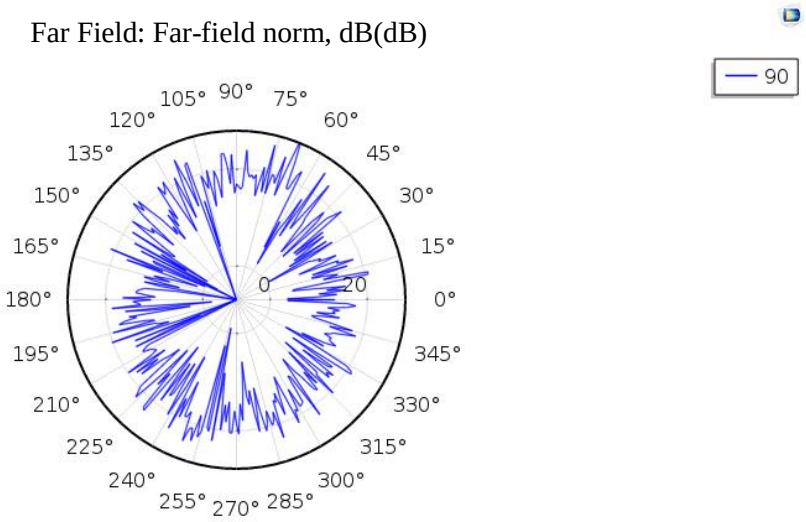

(b) Polar plot point graph with Far Field distribution along r-axis

Figure 4.16: Far Field Simulation for 91°

For 91° of aspect angle, the far field strength result is 14.26472206 dBsm which is certainly better from 87°. The average data is calculated from the 360° values of angle of incidence and r-axis data.

Chapter 5

CONCLUSION AND FUTURE SCOPES

5.1 Introduction

"Study and Performance Analysis of Radar Cross Section for F-117A Nighthawk Stealth Aircraft" concentrates on radar fundamentals, principles and rigorous mathematical derivations. Computer simulation of the radar system performance over measuring radar cross section is of great importance in the initial research and development (R&D) steps of recognition, detection and tracking and in modern radar education. Radar system analysis requires expensive experiments. The task of simulation is to replace such experiments in initial steps.

5.2 Discussion

Chapter 1 discusses evolution of RADAR as a form of technology. The state of radar technology at various periods of history was briefly discoursed. Inception of first military radar, advances made during the world war time and finally state of radar technology in the digital age was discussed. In this chapter, the basic radar system, its classification are also described. In the process, it is shown graphically that increasing the pulse width increases the effective detection range for a pulsed radar system. It is not an economic way to increase the range as it means increasing the transmitted power. However, fine resolution requires pulse width to be as small as possible (or bandwidth as large as possible). Achieving fine range resolution while maintaining adequate average transmitted power can be accomplished by using pulse compression techniques (not part of this thesis).

Basic principle of radar technology, its operational frequency and block diagram of radar system were explained in Chapter 2. In this chapter, the basic equation for a mono-static pulsed radar system is developed. The analysis was extended to find the equation for the bi-static radar system. Then different parameters were varied to observe their effects on the radar range by using MATLAB simulation. Doubling the peak power improves SNR only a little whereas doubling the RCS improves SNR a little better. We also found from

the simulation that we can increase the antenna aperture to compensate for the lack of power being transmitted to cover a wider range area for target detection.

In chapter 3, the methods of RCS calculation are examined. Target RCS fluctuations due to aspect angle, frequency, and polarization are presented. Radar cross section characteristics of some simple and complex targets are also considered. Radar cross section fluctuates as a function of radar aspect angle and frequency. It is evident that RCS fluctuation is more prominent to the variation of frequency. Little frequency change can cause serious RCS fluctuation. Constructive and destructive interference takes place between the RCS of two individual scatterers depending on the aspect angle. Example of backscattered RCS for a number of simple shape objects (such as sphere, circular flat plate, circular cylinder etc.) were presented. The analysis is done for far field mono-static RCS measurements in the optical region.

In chapter 4, simulation result reveals that RCS significantly increases at a particular frequency and in some of specific aspect angles for the F-117A. Consequently, it exhibits better detectability of stealth aircraft in the upper order frequency and at specific aspect angles. The frequency band selection for the simulation has specific purpose. S band is chosen as a precaution for the ground station over any unidentified object which can be detected since the object is within 200 nautical miles at any direction. The shorter wavelengths of the X band allow for higher resolution imagery from high-resolution imaging radars for target identification and discrimination. If there is a radar guided weapon system installed and synchronized, the target object can be destroyed long before it attacks. The aspect angle is varied because of detecting the target with a narrow beam with high power density for higher precision of the target's location whether in bad weather condition. At specific aspect angle, RCS varies significantly. Thus, by setting up the narrow beam at specific aspect angle, the target object can be almost precisely located.

Chapter 5 concluded the experimental work with the possible improvements in radar technology and also future scopes, extensions are discussed here.

5.3 Limitations

Through high performance computer, we created a virtual anechoic chamber and measured the simulated RCS for some parameter variation. During experiment we faced the following limitations:

- Due to unavailability of anechoic chambers practical measurements could not be made.
- We dealt with an open source 2D CAD model of F-117A. With the actual dimensions and measurement 3D CAD model of the same object can be built and simulated with high performance software.
- The adaption of algorithm depends on the simulation target. The very definition for a RF Stealth aircraft is its boresight X-band RCS is smaller than -10 dBsm, which means several dBsm of error is not acceptable.
- Radar Absorbent Material (RAM) was not included in our experiment because simulating RAM is not a trivial matter. RAM includes impedance matching types, resonant material types, circuit analog type, magnetic type and dynamically adaptive types. The mesh resolution must be much smaller than the layer thickness of the RAM to fully reveal its characteristics and this is the real challenge.
- RCS simulation cannot replace actual RCS measurement. The errors of commercial RCS codes usually are around several dBsm depending on situations. A far field outdoor RCS measurement facility build up is the first step towards developing a RF Stealth fighter, and an indoor anechoic room is necessary for near field measurement to verify the effectiveness of surface coatings.

5.4 Future Scopes

In this thesis work, we have studied bi-static radar and stationary target. In most practical radar system, there exists relative motion. So the future concern of the study and analysis could be the dynamic RCS. The study of Moving Target Indicator (MTI) gives a broader scope of future work. Study of antenna RCS reduction is also a prospective field.
If facilities are made available students can be make prototype target objects and carry on research in RCS calculation and improvement in radar technology.

REFERENCES

[1] Radar [Online]

Available:www.britannica.com/EBchecked/topic/488278/radar/28737/First-military-radars

Updated till 18 December, 2017

[2] History of Radar [Online]

Available: http://ethw.org/Radar_during_World_War_II

Updated till 18 December, 2017

[3] FEKO Comprehensive Electromagnetic Solutions [Online]

Available: www.feko.info

Updated till 18 December, 2017

[4] Radar Configurations and Types [Online]

Available: http://opwx.db.erau.edu/faculty/mullerb/Wx365/Radar_components/radar_components.html

Updated till 18 December, 2017

[5] Bassem R. Mahafza. *Radar System Analysis and Design using Matlab*, 2nd edition, Chapman & Hall/CRC, 2000.

[6] Radar Tutorial Website [Online]

Available: http://www.radartutorial.eu/01.basics/rb05.en.html

Updated till 18 December, 2017

[7] The Official Stealth Fighter Handbook [Online]

Available: www.flightsimbooks.com/stealthfighter/01_2_What_Is_Stealth_Technology.php

Updated till 18 December, 2017

[8] The official Airborne Early Warning Association website library [Online]

Available: http://www.aewa.org/Library/rf_bands.html

Updated till 18 December, 2017

[9] Dr. Robert M. O'Donnell, *Introduction to Radar Systems*, MIT Lincoln Laboratory.

[10] M. I Skolnik, *Introduction to Radar Systems*, 3rd edition, McGraw-Hill, 2001

[11] IEEE Standard Definitions of Terms, *IEEE Antenna Standards Committee of the IEEE Antennas and Propagation Society*, Sed 145-1993, The Institute of Electrical and Electronics Engineers, 345 E. 47 Street, New York, USA.

[12] L. Zhu, X. Liang, J. Li, R. Li, 'Simulation analysis on static scattering characteristics of stealth aircraft', *IEEE Advanced Information Management, Communicates, Electronic and Automation Control Conference (IMCEC),* pp. 1774 ~ 1778, Xi'an, China, 2016.

[13] E. F. Knott, J. F. Shaeffer, M. T. Tuley, 'Radar Cross Section', 2nd ed., Norwood, MA: Artech House, 1993.

[14] How to detect Stealth Aircraft [Online]

Available: https://www.defenceaviation.com/2016/05/how-to-detect-stealth-aircraft.html

Updated till 18 December, 2017

[15] F-117A Nighthawk – Military Aircraft [Online]

Available: https://fas.org/man/dod-101/sys/ac/f-117.htm

Updated till 18 December, 2017

[16] F-117A Stealth Fighter replacement and retirement [Online]

Available: http://www.airforce-technology.com/projects/f117/

Updated till 18 December, 2017

[17] COMSOL Comsol [Online]

Available: http://information-technology.web.cern.ch/services/software/comsol

Updated till 18 December, 2017

[18] Comsol Multiphysics [Online]

Available: https://www.comsol.com/

Updated till 18 December, 2017

[19] F-117 Nighthawk [Online]

Available: https://www.lockheedmartin.com/us/100years/stories/f-117.html

Updated till 18 December, 2017

[20] Perfect Electric Conductor [Online]

Available: https://www.electrical4u.com/properties-of-electric-conductor/

Updated till 18 December, 2017

[21] The Perfectly Matched Layer [Online]

Available: https://www.comsol.com/blogs/using-perfectly-matched-layers-and-scattering-boundary-conditions-for-wave-electromagnetics-problems/

Updated till 18 December, 2017

[22] The Impedance Boundary Condition [Online]

Available: Available: https://www.comsol.com/blogs/modeling-metallic-objects-in-wave-electromagnetics-problems/

Updated till 18 December, 2017

[23] Frequency Domain Meshing [Online]

Available: https://www.comsol.com/multiphysics/mesh-refinement

Updated till 18 December, 2017

[24] D.A. White, M. Stowell, 'Full-wave simulation of electromagnetic coupling effects in RF and mixed-signal ICs using time-domain finite-element method', *IEEE Journals & Magazines, Vol. 52, Issue: 5,* pp. 1404 ~ 1413, ISSN 0018 – 9480, USA, May 2004.

[25] Electromagnetic Scattered far-field using Comsol RF Module

Available: http://jice.lavocat.name/blog/2010/04/how-to-get-the-electromagnetic-scattered-far-field-using-comsol-rf-module/

[26] X.-B. Zhou, S.-H. Liu, L.-X. Guo, Y. Xiao, Z.-Y. Li, 'Analysis of RCS of Certain Rough Targets in Terahartz Band', *IEEE 11th International Symposium on Antennas, Propagation and EM Theory (ISAPE),* pp. 727 ~ 730, Guilin, China, 2016.

[27] E. B. Kamel, A. Peden, P. Pajusco, 'RCS modeling and measurements for automotive radar applications in the W band', *IEEE 11th European Conference, Antennas and Propagation (EUCAP),* pp. 2445 ~ 2449, Paris, France, 2017.

[28] G. Mollo, R. D. Napoli, G. Naviglio, C. D. Chiara, E. Capasso, G. Alli, 'Multifrequency Experimental Analysis (10 to 77 GHz) on the Asphalt Reflectivity and RCS of FOD Targets', *IEEE Geoscience and Remote Sensing Letters, Vol. 14, Issue: 9, no.14,* pp. 1441 ~ 1443, Naples, Italy, September 2017.

[29] H. El-Kamchouchy, K. Saada, A. E.-D. S. Hafez, 'An Accurate Multistatic Radar RCS (MRCS) for Airhawk F117 Stealthy Target', *IEEE Computer Modelling and Simulation (UKSim),* pp. 734 ~ 738, Cambridge, UK, 2013.

[30] M. A. Alves, R. J. Port, M. C. Rezende, 'Simulations of the radar cross section of a stealth aircraft', *IEEE Microwave and Optoelectronics Conference, IMOC, SBMO/IEEE MTT-S International*, pp. 409 ~ 412, Brazil, 2007.

[31] A. David, C. Brousseau, A. Bourdillon, 'Simulations and measurements of a radar cross section of a Boeing 747–200 in the 20–60 MHz frequency band', *IEEE American Geophysical Union (AGU), Radio Science, Vol. 38, Issue: 4, no.38,* pp. 3-1 ~ 3-4, August 2003.

[32] C. W. Trueman, S.J. Kubina, S.R. Mishra, C. L. Larose, 'RCS of Small Aircraft At HF Frequencies', *IEEE Symposium on Antenna Technology and Applied Electromagnetics[ANTEM]*, pp.151 ~ 157, Ottawa, Canada, August 1994.

[33] E. Kemptner, D. Klement, H. Wagner, 'RCS Determination for DLR Stealth Design F7', *RTO, SCI Symposium,* Germany, 1998.

[34] J.W. Coltman, "The Scintillation Counter", *Proceedings of the IRE, Vol: 37, Issue: 6,* pp. 671 ~ 682, ISSN: 0096 – 8390, East Pittsburg, June 1949.